NASA TECHNICAL NOTE

NASA TN D-7695

NASA TN D-7695

THE APPLICATION OF ACOUSTIC EMISSION TECHNIQUE TO FATIGUE CRACK MEASUREMENT

by Jag J. Singh, William T. Davis, and John H. Crews, Jr.

Langley Research Center
Hampton, Va. 23665

NATIONAL AERONAUTICS AND SPACE ADMINISTRATION • WASHINGTON, D. C. • OCTOBER 1974

1. Report No. NASA TN D-7695	2. Government Accession No.	3. Recipient's Catalog No.
4. Title and Subtitle THE APPLICATION OF ACOUSTIC EMISSION TECHNIQUE TO FATIGUE CRACK MEASUREMENT		5. Report Date October 1974 6. Performing Organization Code
7. Author(s) Jag J. Singh, William T. Davis, and John H. Crews, Jr.		8. Performing Organization Report No. L-9530
9. Performing Organization Name and Address NASA Langley Research Center Hampton, Va. 23665		10. Work Unit No. 501-22-02-02 11. Contract or Grant No.
12. Sponsoring Agency Name and Address National Aeronautics and Space Administration Washington, D.C. 20546		13. Type of Report and Period Covered Technical Note 14. Sponsoring Agency Code
15. Supplementary Notes		

16. Abstract

The applicability of acoustic emission technique to measure fatigue cracks in aluminum alloy specimens has been investigated. It has been shown that a $\Sigma N \propto K^m$ type of acoustic emission law can be applied to the slow crack growth region $\left(\frac{da}{dn} < 25 \times 10^{-4} \text{ mm/cycle}\right)$ and may be used to verify the crack length changes. However, there are several variables, such as the metallurgical and the physical treatment of the specimen, that can affect the level of acoustic activity of a fatigue specimen. It is therefore recommended that the acoustic emission technique be supplemented by other nondestructive evaluation methods to obtain quantitative data on crack growth.

17. Key Words (Suggested by Author(s)) Nondestructive evaluation Acoustic emission Flaw detection Fatigue damage	18. Distribution Statement Unclassified – Unlimited STAR Category 15		
19. Security Classif. (of this report) Unclassified	20. Security Classif. (of this page) Unclassified	21. No. of Pages 40	22. Price* $3.25

For sale by the National Technical Information Service, Springfield, Virginia 22151

THE APPLICATION OF ACOUSTIC EMISSION TECHNIQUE TO FATIGUE CRACK MEASUREMENT

By Jag J. Singh, William T. Davis, and John H. Crews, Jr.
Langley Research Center

SUMMARY

The applicability of acoustic emission technique to measure fatigue cracks in aluminum alloy specimens has been investigated. It has been shown that a $\Sigma N \propto K^m$ type of acoustic emission law can be applied to the slow crack growth region $\left(\frac{da}{dn} < 25 \times 10^{-4} \text{ mm/cycle}\right)$ and may be used to verify the crack length changes. However, there are several variables, such as the metallurgical and the physical treatment of the specimen, that can affect the level of acoustic activity of a fatigue specimen. It is therefore recommended that the acoustic emission technique be supplemented by other nondestructive evaluation methods to obtain quantitative data on crack growth.

INTRODUCTION

Fatigue cracks initiate early in the life of high strength structural materials used in aerospace industry. Most of the useful life of components made from such materials is spent in the crack growth phase of fatigue. Consequently, more efficient nondestructive evaluation methods of inspection should be developed to determine the remaining useful life of these components. In several recent studies (refs. 1 to 3), it has been reported that the acoustic emission technique is superior to other techniques, such as radiography, ultrasonics, or magnetic particle inspection – particularly in the case of tight cracks. However, most of the previous studies (refs. 4 to 5) have been confined to large crack growth rates $\left(>25 \times 10^{-4} \text{ mm/cycle}\right)$ which are encountered toward the end of the useful life of most structural components. Recently, Harris and Dunegan (ref. 6) have studied continuous monitoring of fatigue crack growth rates of less than one millionth of a centimeter per cycle by acoustic emission techniques. Their results indicate that the acoustic emission technique may be suitable for measuring slow crack growth rates in cyclically loaded structures. In the present report, the acoustic emission technique is evaluated for thin plate specimens with slowly growing cracks $\left(<25 \times 10^{-4} \text{ mm/cycle}\right)$. Principal correlations are established between the acoustic emissions (resulting from the release of energy, accompanying processes of deformation and fracture under static and cyclic loading) and crack tip stress intensity factor K. These correlations are used to predict the crack extensions in specimens undergoing fatigue loading. The predicted values of the crack extension are compared with the measured values.

SYMBOLS

$2a$	total crack length (In case of center-notched specimen, it includes the notch length.)
D	acoustic emission constant of proportionality
$\frac{da}{dn}$	crack half-length extension per fatigue cycle
K	stress intensity factor for static loading
ΔK	stress intensity factor range in tension-tension cyclic loading, $K_{max} - K_{min}$
K_f	stress intensity factor at final proof overload
K_i	stress intensity factor at initial proof overload
m	numerical constant, equal to exponent of K (or ΔK) in relation of N as a function of K (or ΔK)
ΔN	acoustic counts during proof test
ΣN	cumulative acoustic emission counts
$\frac{dN}{dn}$	acoustic emission rate per fatigue cycle
$\frac{dN}{dt}$	acoustic emission rate
n	number of fatigue cycles
R	stress ratio, $\frac{\sigma_{min}}{\sigma_{max}}$
r_y	radius of plastic zone at crack tip
σ	applied stress
σ_p	periodic proof stress
σ_w	working stress during fatigue $(\sigma_w < \sigma_p)$

Subscripts:

f	final
i	initial
max	maximum
min	minimum

BASIS OF ACOUSTIC EMISSION TECHNIQUE

In the last quarter of a century, more and more mechanical and structural complexes based entirely on static strength concepts have been found to have an insufficient margin of safety. Metal fatigue, resulting from dynamic processes in the materials, has been increasingly recognized as a principal cause of failure. It is now generally believed that the application of cyclic stress causes the movement of ever-present dislocations and defects in the test structures. These defects or dislocations pile up at the imperfections, such as grain boundaries and interphase interfaces, or at impurities in the material. As the stress cycling is continued, some of these defects or dislocations break away and continue their way to other potential barriers where they will accumulate until they break away again, or until localized material failure occurs. Both of these phenomena, breakaway of dislocations or defects from the grain boundaries and localized yielding of the material, are accompanied by the release of stress waves which travel through the material in all directions. These stress waves appear as compressional or shear waves on the specimen surface and constitute the source of the acoustic emission signal. Such a signal is transient, contains several frequencies, and cannot, in general, be described by an explicit mathematical expression. The signal arriving at the receiver may be approximated by an expression of the form

$$A(x,t) = \sum_i A0_i e^{-k_i x} \sin(\omega_i t + \varphi_i) \quad , \tag{1}$$

where

$A0_i$	initial wave amplitude of ith component
k_i	attenuation factor for ω_i
ω_i	frequency of ith stress wave
x	"source" to transducer distance

t transit time from source to transducer

φ_i phase angle of ith component

Clearly, A(x,t) is time dependent and will be nonzero only when waves arrive at the receiver from the primary event that released the stress energy. The frequencies of these acoustic waves are not characteristic or unique. For example, a 0.125-mm grain in a polycrystalline material with a shear modulus $G = 2.76 \times 10^4$ MN/m^2, when suddenly shocked by a slip event in the material, begins to resonate at approximately 2 MHz. If the grain is regarded as a bubble, the pulsating frequency will be approximately 50 MHz. A trapped stress wave will cause the bubble to oscillate to about 25 MHz. (See ref. 1.) A microscopic event in a fatigue specimen acts like a sudden impulse which generates, in most random polycrystalline materials, a series of frequencies ranging from audible to several megacycles. (The finite size of the test specimen tends to modify the original acoustic emission spectrum.) This observation is supported by the experimental evidence that transducers with mounted resonance frequencies from 10 kHz to 30 MHz have been excited. (See ref. 7.)

Once a crack has developed in the specimen, energy release associated with the plastic zone at the crack tip dominates the acoustic emission phenomenon. Under these circumstances, the total number of stress waves released can be related to the crack size. The dimension of the plastic zone r_y at the tip of a plane-strain crack is related to the opening mode stress intensity factor K as follows (ref. 8):

$$r_y = \frac{1}{4\sqrt{2\pi}}\left(\frac{K}{\sigma_y}\right)^2 \tag{2}$$

where σ_y = Yield stress of the test material. In the case of through cracks in thin plate specimen the volume of the plastic zone (based on eq. (2)), and hence the number of acoustic emission signals ΣN produced, should be proportional to K^4. As indicated earlier, the stress waves have a continuous spectrum of frequencies. If these stress waves are detected at a "single" frequency and at a fixed distance from the "source," the dependence of ΣN and K may be different from the fourth power. Furthermore, such a relation need not be unique for all types of tests, since it is expected to depend upon the nature and history of the material, the stress-wave frequency spectrum, the mounted resonance frequency of the stress-wave detector, the discriminator threshold in the counting system, and, possibly, the frequency bandwidth selected.

The acoustic emission data may be used in several ways to obtain information about the crack(s). For example, by using the experimentally determined correlation function between ΣN and K and assuming the validity of Kaiser effect (ref. 9), according to which acoustic emissions are not generated during a reloading of the material unless the stress intensity factor exceeds its previous high level, it is possible to determine K as follows.

Let the experimental correlation function between ΣN and K be of the following form (ref. 3):

$$\Sigma N = DK^m \tag{3}$$

Then

$$\Delta N = \int_{K_i}^{K_f} \frac{dN}{dK}\, dK \tag{4a}$$

$$\Delta N = D\left(K_f^m - K_i^m\right) \tag{4b}$$

where K_i and K_f are the stress intensity factors in the two consecutive periodic proof tests and ΔN represents the acoustic counts observed when K changes from K_i to K_f. Rearranging equation (4b),

$$\Delta N = DK_i^m\left[\left(\frac{K_f}{K_i}\right)^m - 1\right] \tag{5}$$

Thus, an experimental determination of ΔN, coupled with a knowledge of m and K_i, is expected to provide information about the final value of the stress intensity factor K_f and, hence, the final crack length a_f. From equation (5),

$$K_f = \left(K_i^m + \frac{\Delta N}{D}\right)^{1/m} \tag{6}$$

For a center-notched specimen of the type used in the present study, $K_f = \sigma_f\left(\sqrt{\pi a_f}\right)\alpha_f$, where α_f is the crack size correction term.[1] Equation (6) can be rearranged as follows:

$$a_f = \frac{1}{\pi\sigma_f^2\alpha_f^2}\left[\left(\sigma_i\sqrt{\pi a_i}\alpha_i\right)^m + \frac{\Delta N}{D}\right]^{2/m} \tag{7}$$

An alternative technique would involve measuring acoustic emission rate dN/dn over several cycles at proof stress σ_f. Then using the experimentally determined calibration relation dN/dn plotted against ΔK, one is able to determine the corresponding ΔK and hence the final crack length. However, the scatter in the data usually encountered in acoustic emissions studies may make it difficult to obtain a "true" proof dN/dn value.

EXPERIMENTAL PROCEDURE

Thin aluminum sheet specimens (fig. 1) were used in the present investigation. These specimens were fabricated from 2.28-mm-thick 7075-T6 and 2024-T3 aluminum alloy sheets. The acoustic emission signals were detected with highly sensitive lead-zirconium-titanate (PZT) piezoelectric transducers attached to the tensile specimen with silicone rubber cement. The transducers were located 2.54 cm from the notch, the anticipated site for acoustic emission, in order to minimize the effects of reflection at the specimen boundaries. The acoustic signals are transient and produce a damped sinusoidal wave in the transducer with a characteristic frequency equal to its mounted resonant frequency. The resonance frequencies of the transducers ranged from 100 kHz to 1.5 MHz. The transducer characteristics are summarized in table I. Frequencies higher than 1.5 MHz were not investigated because of high signal attenuation with distance expected at higher frequencies. The transducer signal, after conditioning by a

---

[1]For center-notched specimen, the stress intensity factor K is calculated from the following expression (ref. 10):

$$K = 1.77\sigma(a)^{1/2}\left(1 - 0.1\lambda + \lambda^2\right)$$
$$= 1.25\sigma\sqrt{2a}\left(1 - 0.1\lambda + \lambda^2\right)$$

In this expression,

σ	applied tensile stress
2a	total crack length
λ	crack length/specimen width

For λ up to 0.7, the accuracy of the compact expressions is better than 1 percent.

fixed gain, low-noise preamplifier (40-dB gain; 50-kHz to 5-MHz bandwidth), was further amplified in a variable-gain (up to 60 dB) amplifier containing four selectable filters. (See table II.)

TABLE I.- SUMMARY OF PIEZOELECTRIC TRANSDUCER CHARACTERISTICS

Nominal resonance frequency	Type of connector	Type of transducer	Sensitivity re 1V/μbar	Physical size
150 kHz	BNC	Single ended	-80 dB	1.9-cm diam × 2.5 cm
1.50 MHz	Microdot	Differential	-85 dB	1.9-cm diam × 2.9 cm
100 kHz	Microdot	Single ended	(1 mV/g)*	0.95-cm diam × 0.95 cm

*This is more than one order of magnitude below the sensitivity of the 150-kHz acoustic transducer. All sensors were provided with a 1.5-mm insulating shoe to prevent electrical contact with the test specimen.

TABLE II.- SUMMARY OF INTERNAL FILTER BANDWIDTHS IN THE AMPLIFIER

Filter selection	Frequency at -3 dB	Frequency at -5 dB
1	200 to 230 kHz	180 to 255 kHz
2	100 to 400 kHz	90 to 450 kHz
3	0.50 to 2.00 MHz	0.45 to 2.30 MHz
4	0.1 to 3.00 MHz	0.09 to 3.50 MHz
5	Continuously adjustable from 10 kHz to 200 kHz; used at 80 to 150 kHz at -3 dB for the 100-kHz transducer.	

By properly selecting the internal filter, the amplifier output can be confined to a relatively narrow band of frequencies containing the transducer resonance frequency. These narrowly banded signals, after passing through an adjustable fast discriminator, were counted with a fast scaler-timer. By adjusting the discriminator level until the counter just became quiescent, it was possible to minimize the effects of the background and system noise.

The acoustic emission event is an impulse phenomenon and has a duration of the order of 0.01 microsecond or less. (See ref. 1.) Consequently, the acoustic transducer is shocked into ringing by such an event. The number of oscillations counted by the system during each event is determined by the event amplitude and the discriminator threshold. For the detected acoustic emission to correlate closely with the released strain energy, as many ring-down cycles should be counted as possible. However, those smaller than the discriminator threshold, which must be set above the system noise level, cannot be counted. This fact explains why a good acoustic emission system must

have very low electrical noise (less than an equivalent of a few microvolts at the pre-amplifier input). The present system met these requirements. To minimize the effects of discriminator level drift and system gain changes, the discriminator level was set to twice the overall system noise level.

The test specimens were mounted in a closed loop, servo-controlled hydraulic test machine using friction grips and subjected to static as well as cyclic loading. The pump cavitation and background noise, as observed in the case of uncracked specimen under low cyclic and static stresses, did not contribute to the counts recorded, mainly because of the high resonant frequency of the acoustic transducer and careful mounting of the fatigue specimen. The friction grip surfaces were replaced after each use. A complete block diagram of the experimental setup is shown in figure 2. Figure 3 shows a photograph of the test machine, with the tensile specimen mounted in it, and the associated counting electronics.

The acoustic emission signals measured with the test specimen under various types of loading (static, cyclic or cyclic-static) were recorded and computer analyzed. The propagating crack lengths in the test specimen were measured by using × 10 microscopes and synchronized stroboscopic illumination. By using the data on crack lengths and the accompanying acoustic emissions, functional relations between these observables were established by use of fracture mechanics concepts. Using the analytical expressions thus obtained, several static proof tests were conducted to evaluate the acoustic emission technique for predicting crack extensions. The proof-test sequence consisted of subjecting an unflawed test specimen to cyclic loads in the stress range $(\sigma_1$ to $\sigma_2)$ until a crack of length $2a$ (approximately 0.5 cm) was developed. The summation acoustic emission N_1 during this time was recorded. The cyclic loading was stopped for a period of 1 minute during which the specimen was left at a static load of σ_2. The specimen was then subjected to a static load of $\sigma_3 = 1.5\sigma_2$ for a period of 2 minutes. This loading constituted the first proof loading. During this loading at σ_3, the acoustic emission ΔN_1 and any changes in crack length were recorded. The static load was removed and the specimen was again subjected to cyclic loading in the range $(\sigma_1$ to $\sigma_2)$ for a period of 2 minutes. During this period, the acoustic emission signals were continuously recorded. The cyclic loading was stopped and the specimen subjected to static loading at σ_2 for a period of 1 minute. During this waiting period at σ_2, the crack length was measured. The specimen was then subjected to a static load of σ_3 for a period of 2 minutes. This loading constituted the second proof load. During this loading, the acoustic emissions ΔN_2 and any crack length changes were recorded. This sequence was continued until the specimen failed. From the proof test counts ΔN the crack length was computed by using the previously established relation between ΔN and K. The computed crack lengths were compared with the measured crack lengths to evaluate the acoustic emission technique for fatigue crack growth measurement.

EXPERIMENTAL RESULTS AND DISCUSSION

The results of experiments conducted on center-notched 2024-T3 Al specimen by use of a 150-kHz transducer are discussed. The results for 7075-T6 Al specimens are essentially like those for 2024-T3 Al. The specimen type and the resonance frequency of the piezoelectric transducer did not affect the form of the relations between the various measurables. All measurements were conducted at room temperature and in ambient air. No attempt was made to locate the crack during the present study, although it could have been found easily by standard triangulation techniques.

Acoustic Emission Observed Under Static Loading

Figure 4 shows the summation acoustic counts as a function of the applied static stress from two initially uncracked specimens. For these tests, the static loading was increased in preselected increments and held for 30 seconds at each step while the acoustic signals were counted. There are two types of acoustic emission signals observed under such circumstances (refs. 1 and 3): first, low-level continuous components associated with plastic deformation at low strain; and secondly, high-level bursts, randomly produced, associated with microcrack formation or extension.

From the type of data shown in figure 4, the acoustic emission rates dN/dt were computed as a function of the applied load. Typical results are shown in figure 5. The acoustic emission activity is clearly reduced just before the specimen fails. It may be due to the cessation of low-level acoustic activity at higher strain. (See ref. 11.)

Figure 6 shows acoustic emission from an initially cracked specimen during a monotonically increasing load. Notice the difference between figures 4 and 6. The onset of high-level bursts (associated with crack extension) at applied stress levels of 208 MN/m^2, 254 MN/m^2, 286 MN/m^2, and 318 MN/m^2 is indicated in figure 6. Figure 7(a) summarizes the data ΣN plotted as a function of σ for a number of flawed 2024-T3 Al specimens subjected to increasing static loads. The plots in this figure show considerable scatter even when the specimen had similar initial flaws. Figure 7(b) shows the same data plotted against the corresponding stress intensity factor K. Although there is considerable scatter, the individual curves appear to resemble one another slightly better than the curves in figure 7(a) do. This result is expected since the plastic deformation at the crack tip, believed to be the source of acoustic emission, is controlled by K. (See ref. 3.)

A relationship between the observed acoustic emission and the physical parameters associated with the internal conditions in the test specimen will now be established. The experimentally observed cumulative acoustic emission counts ΣN are a function of the stress intensity factor K. Figures 8(a) and 8(b) show the dependence of summation

acoustic emission on the stress intensity factor in the case of two specimens with different initial flaws loaded statically to failure. In both instances, the data fit an expression of the form:

$$\left(\Sigma N - \Sigma N_0\right) \propto K^m \qquad (m = 2.55 \pm 0.15) \qquad (8)$$

where ΣN_0 indicates cumulative acoustic emission until a through crack first developed in the specimen. (The initial flaws were produced in the specimen by cyclic loading at low stress levels.) All counts associated with microcrack formation, surface embedded flaws as well as any background noise, are included in ΣN_0. Figure 8 clearly shows that there is a close relation between the stress energy released proportional to ΣN and the stress intensity factor K.

Acoustic Emission Observed Under Cyclic Loading

Figure 9 shows acoustic emission measured for an initially unflawed 2024-T3 Al specimen subjected to cyclic loading at 5.2 to 160 MN/m^2 at 16 Hz. Notice the difference between this figure and figure 4. In the case of cyclic loading, the summation acoustic emission continues to rise monotonically until fracture occurs.

A comparison between ΣN and an eddy probe bridge output from a specimen subjected to cyclic loading at 5.2 to 104 MN/m^2 at 16 Hz is shown in figures 10(a) and 10(b). These data were taken with a double-edge notched specimen for the convenience of using an eddy probe. The specimen configuration, however, is not expected to affect the observed correlation between the acoustic emission and the eddy probe data. After crack initiation, the acoustic counts as well as the eddy bridge output increased nearly with the fatigue cycles. It is clear from these two figures that the acoustic emission and the eddy current signals are associated with the same dynamic processes in the test specimen, namely, the crack extension in the specimen. Figure 11(a) summarizes data for ΣN plotted as a function of $2a$ observed when the unflawed 2024-T3 Al specimens were cyclically loaded at two different stress ratios. Like figure 7, the data in this figure also show considerable scatter even when the external factors are kept constant. It is important to remember these differences since supposedly identical specimens do not exhibit the same degree of acoustic activity; this result is probably due to differences in their internal structure or previous mechanical history. The acoustic emission data in figure 11(a) are replotted against the stress intensity factor range ΔK in figures 11(b) to 13. A comparison of figures 12 and 13 suggests that the correlation of ΣN with ΔK is not affected by the magnitude of the cycling stress, within the accuracy of the present measurement.

Figure 14(a) shows the dependence of $\left(\Sigma N - \Sigma N_0\right)$ on ΔK for an initially uncracked specimen cycled under tension-tension loading to failure. Figure 14(b) shows a similar

result at a slightly different cyclic stress ratio. In both instances, the data appear to fit an expression of the following type:

$$(\Sigma N - \Sigma N_o) \propto (\Delta K)^m \qquad (m = 2.5 \pm 0.1) \qquad (9)$$

where ΣN_o has the same significance as in equation (8).

Once a crack has developed in a specimen subjected to cyclic loading, crack closure can present an unwanted acoustic source. This condition can occur even in a tension-tension cycle such as the one used in the present study. Figure 15 shows oscilloscope traces of the load cycle, crack closure signal (in the unloading half of the load cycle), and the acoustic emission burst (near the maximum load). It is evident that in the present study the amplitude of crack closure noise signals is much lower than that of the acoustic emission signals associated with the crack extension. Either by a proper selection of the discriminator level in the counting system or by counting only in the maximum half of the load cycle, the crack closure counts can be eliminated without appreciably affecting the acoustic data. The former procedure was used in the present study. (It should be noted that the removal of stress during the decreasing part of the stress cycle may result in backup of dislocations against the residual stress, leading to acoustic emission. However, the amplitude of dislocation arrest-related signals is usually much lower than the amplitude of the crack propagation related signals. Thus, perhaps the amplitude discrimination, rather than the load-signal time correlation, would be more appropriate for excluding signals other than those associated with the crack propagation.) The similarity of the data in figures 8 and 14 shows that the acoustic emission activity in cracked specimens is related to the increase in K or ΔK (and the accompanying plasticity), rather than the cause of that increase, whether cyclic or tensile loading. This conclusion is further exemplified by the discussion of figures 16 to 18.

Figure 16 shows the crack propagation rate in 2024-T3 Al specimens subjected to cyclic loading in the range 5.2 to 186 MN/m^2 at 13 Hz. The crack extends at a faster rate as it grows larger. This behavior is further illustrated in figure 17 where the data show that the observed dependence of the crack extension rate da/dn on the crack length $2a$ is of the form:

$$\frac{da}{dn} \propto (2a)^{1.1}$$

More extensive data indicate that $\frac{da}{dn} \propto (2a)^{1.2\pm0.1}$ for thin-plate specimens. The expected values of crack length exponent range from 1 (refs. 12 and 13) to 2 (ref. 14). Since it is the stress intensity factor rather than the crack size that controls the onset of rapid crack propagation (refs. 10 and 15), the da/dn values should be plotted against the corresponding ΔK values. This plotting has been done in figure 18. To illustrate further the importance of ΔK in crack growth rates da/dn as a function of ΔK has

been calculated from da/dn as a function of 2a data for several stress ratios. Figure 19 shows da/dn as a function of ΔK at two stress ratios. Within the accuracy of the present measurements, the da/dn values correlate with the ΔK values. Figure 20 summarizes similar results for several stress ratios.

The crack extension rate da/dn shows the same kind of dependence on ΔK as $(\Sigma N - \Sigma N_o)$ does in figure 14. The significance of this result can be appreciated by examining figure 21(a) where dN/dn is plotted against da/dn. It appears that dN/dn and da/dn are almost linearly related functions. Thus dN/dn, like da/dn, is expected to increase as a crack grows. Figure 21(a) also suggests that the correlation between dN/dn and ΔK is expected to be similar to that between da/dn and ΔK as borne out by the data shown in figure 21(b). The dependence of dN/dn on ΔK is expected to be of the form:

$$\frac{dN}{dn} \propto (\Delta K)^{2m-2}$$

These results indicate that the acoustic emission is produced only when the crack changes in size or shape, and that the acoustic emission rate increases as the crack grows. Analytically, the acoustic emission data fit the following expression:

$$\Sigma N = DK^{2.5\pm0.5} \tag{10}$$

Results from this study indicate that for

$$\frac{da}{dn} = 0.0001 \text{ to } 0.0050 \text{ mm/cycle}$$

and

$$\Delta K = 5 \text{ to } 25 \frac{MN}{m^2} \cdot m^{1/2}$$

$$\Sigma N \propto (K \text{ or } \Delta K)^{2.5\pm0.5} \tag{11}$$

for $R \leq 0.1$ where $R = \frac{\sigma_{min}}{\sigma_{max}}$ in the case of cyclic loading in the tension-tension mode.

The acoustic activity described by equations (10) and (11) is considerably weaker than that reported in reference 3 where the power of K or ΔK varied from 4 to 8. This difference is the result of the range of K or ΔK values where the experimental data are taken. Figure 22(a) shows a comparison of experimental fatigue crack growth rates with the predictions of the widely used Paris relation (ref. 14). (These data were taken from ref. 16 where the test conditions, including the test specimen material and the geometrical configuration, were similar to those in the present study.) Notice the data in the following ranges of variables:

$$\Delta K = (5 \text{ to } 20) \frac{MN}{m^2} \cdot m^{1/2}$$

$$\frac{da}{dn} = (0.0001 \text{ to } 0.0050)\ \text{mm/cycle}$$

Figure 22(b) shows these data on an expanded scale. Clearly, the data would fit better with the ΔK exponent in the range 2.4 to 3.0 than for 4 used in the Paris equation. This analysis suggests that one should experimentally determine a crack propagation law for his specific case instead of using a "universal law" for a wider range of data. This determination is necessary because of the correlation between da/dn and dN/dn discussed earlier. The form of $\Sigma N = DK^m$ is expected to depend on the relationship between dN/dn and ΔK.

Proof Testing of the Specimen

The problem of determining the crack length on the basis of observed acoustic emission counts during a static proof overload of a specimen which had a crack of known length before use is discussed. (The alternate technique involving the correlation between dN/dn and ΔK is not described since ΔK and the final crack length are not necessarily uniquely related and it is not expected to give better results than the technique described here.) Recall that the acoustic emission activity is irreversible (Kaiser effect, ref. 9); that is, the acoustic emissions are not generated during the reloading, unless the stress intensity factor exceeds its previous high level. Let K_i correspond to the initial stress intensity factor for a proof stress of σ_p. If the specimen is fatigued enough, at a stress σ_w where $\sigma_w < \sigma_p$, to cause the crack to extend and then loaded again to the proof stress σ_p (corresponding to the final stress intensity factor K_f), a certain number of acoustic emission counts ΔN are observed. Realizing that ΔN, K_i, and K_f are related (eq. (5)), ΔN and K_i can be used to determine K_f. Then K_f can be used to determine the final crack length. (The proof acoustic emission is associated with the creation of a new plastic zone at the crack tip. Hence, the new plastic zone must be ahead of the preceding plastic zone, but the K value during the regular fatigue loading must not exceed K_i if eq. (5) is to be applicable. In the present study, this was insured to be the case.) The results of a typical proof test are shown in figures 23(a) to 23(c). Although the acoustic data in figures 23(a) and 23(b) have a large scatter, the observed relation between ΔN and K_i agrees well with equation (5). A perfect agreement would require all the data points to lie on the solid line in figure 23(a). Figure 23(c) shows a comparison between the measured and the calculated crack lengths, which agree to within 10 percent. In view of the observed data scatter and the lack of data reproducibility, it is concluded that the acoustic emission technique cannot always predict crack growth accurately. This technique does, however, provide reliable indications of changes in the crack length. Furthermore, by combining static and dynamic proof testing, the growth of a crack to critical size can be predicted and catastrophic failure averted.

CONCLUDING REMARKS

The acoustic emission activity from cracked and uncracked aluminum fatigue specimens has been studied under various types of loadings. Emphasis has been placed on fatigue crack growth in the slow growth range, less than 0.0025 mm/cycle. As a result of these studies, the following general conclusions have been drawn.

The validity of the $(\Sigma N \propto K^m)$ relation between N and K in fatigue studies has been demonstrated by the observed correlations amongst the various variables.

Acoustic emission techniques give a reliable indication of changes in the crack dimensions over short periods of time. The level of acoustic activity also indicates the severity of the cracks. However, large variations in acoustic emissions from supposedly identical fatigue specimens make it difficult to measure cracks precisely. Nevertheless, acoustic emission information used with other testing techniques (ultrasonic, radiographic, etc.) can provide a quantitative measure of the fatigue crack length.

In the present study, crack propagation and acoustic emission laws were found to be of the form:

$$\frac{da}{dn} \propto (\Delta K)^m \qquad (m = 2.5 \pm 0.5)$$

$$\frac{dN}{dn} \propto (\Delta K)^{2m-2}$$

where da/dn is the crack half-length per fatigue cycle, dN/dn is the acoustic emission rate per fatigue cycle, and ΔK is the stress intensity factor range in tension-tension cyclic loading. (There are several variables, such as the metallurgical and the physical treatment of the specimen, that can affect the acoustic activity of a fatigue specimen. Consequently, even with a knowledge of the acoustic emission laws, the variation in the proof test counts can prevent an accurate determination of final crack length.)

The agreement between the computed and the measured crack lengths indicates that the Kaiser effect is a valid phenomenon over short periods of time. However, the validity of this phenomenon over extended periods of time, and hence the usefulness of the acoustic emission technique, remains to be confirmed.

Langley Research Center,
National Aeronautics and Space Administration,
Hampton, Va., June 18, 1974.

REFERENCES

1. Liptai, R. G.; Harris, D. O.; Engle, R. B.; and Tatro, C. A.: Acoustic Emission Techniques in Materials Research. Int. J. Nondestruct. Test., vol. 3, no. 3, Dec. 1971, pp. 215-275.

2. Corle, Richard R.; and Schliessmann, Judith A.: Flaw Detection and Characterization Using Acoustic Emission. Mater. Evaluation, vol. XXXI, no. 6, June 1973, pp. 115-120.

3. Dunegan, H. L.; Harris, D. O.; and Tatro, C. A.: Fracture Analysis by Use of Acoustic Emission. Eng. Fracture Mech., vol. 1, no. 1, June 1968, pp. 105-122.

4. Hartbower, C. E.; Gerberich, W. W.; and Liebowitz, H.: Investigation of Crack-Growth Stress-Wave Relationships. Eng. Fracture Mech., vol. 1, no. 2, Aug. 1968, pp. 291-308.

5. Gerberich, W. W.; and Hartbower, C. E.: Some Observations on Stress Wave Emission as a Measure of Crack Growth. Int. J. Fracture Mech., vol. 3, no. 3, Sept. 1967, pp. 185-192.

6. Harris, D. O.; and Dunegan, H. L.: Continuous Monitoring of Fatigue Crack Growth by Acoustic Emission Techniques. Tech. Rep. DE-73-2, Dunegan/Endevco, Feb. 1973.

7. Hutton, P. H.; and Ord, R. N.: Acoustic Emission. Research Techniques in Nondestructive Testing, R. S. Sharpe, ed., Academic Press, Inc., 1970, pp. 1-30.

8. McClintock, F. A.; and Irwin, G. R.: Plasticity Aspects of Fracture Mechanics. Fracture Toughness Testing and Its Applications, Spec. Tech. Publ. No. 381, Amer. Soc. Testing Mater., c.1965, pp. 84-113.

9. Kaiser, J.: Erkenntnisse und Folgerungen aus der Messung von Geraeuschen bei Zugbeanspruchung von metallischen Werkstoffen. Arch. Eisenhuettenwesen, vol. 24, no. 1-2, Jan.-Feb. 1953, pp. 43-45.

10. Brown, William F.; and Srawley, John E.: Plane Strain Crack Toughness Testing of High Strength Metallic Materials. Spec. Tech. Publ. No. 410, Amer. Soc. Testing Mater., c.1966.

11. Dunegan, H. L.; and Green, A. T.: Factors Affecting Acoustic Emission Response From Materials. Acoustic Emission, Spec. Tech. Publ. 505, Amer. Soc. Testing Mater., c.1972, pp. 100-113.

12. Liu, H. W.: Fatigue Crack Propagation and Applied Stress Range – An Energy Approach. Trans. ASME, Ser. D: J. Basic Eng., vol. 85, no. 1, Mar. 1963, pp. 116-122.

13. Liu, H. W.: Crack Propagation in Thin Metal Sheet Under Repeated Loading. Trans. ASME, Ser. D: J. Basic Eng., vol. 83, no. 1, Mar. 1961, pp. 23-31.

14. Paris, Paul C.: The Fracture Mechanics Approach to Fatigue. Fatigue – An Interdisciplinary Approach, John J. Burke, Norman L. Reed, and Volker Weiss, eds., Syracuse Univ. Press, 1964, pp. 107-132.

15. Srawley, John E.; and Brown, William F., Jr.: Fracture Toughness Testing Methods. Fracture Toughness Testing and Its Applications, Spec. Tech. Publ. No. 381, Amer. Soc. Testing Mater., c.1965, pp. 133-198.

16. Hudson, C. Michael: Effect of Stress Ratio on Fatigue-Crack Growth in 7075-T6 and 2024-T3 Aluminum-Alloy Specimens. NASA TN D-5390, 1969.

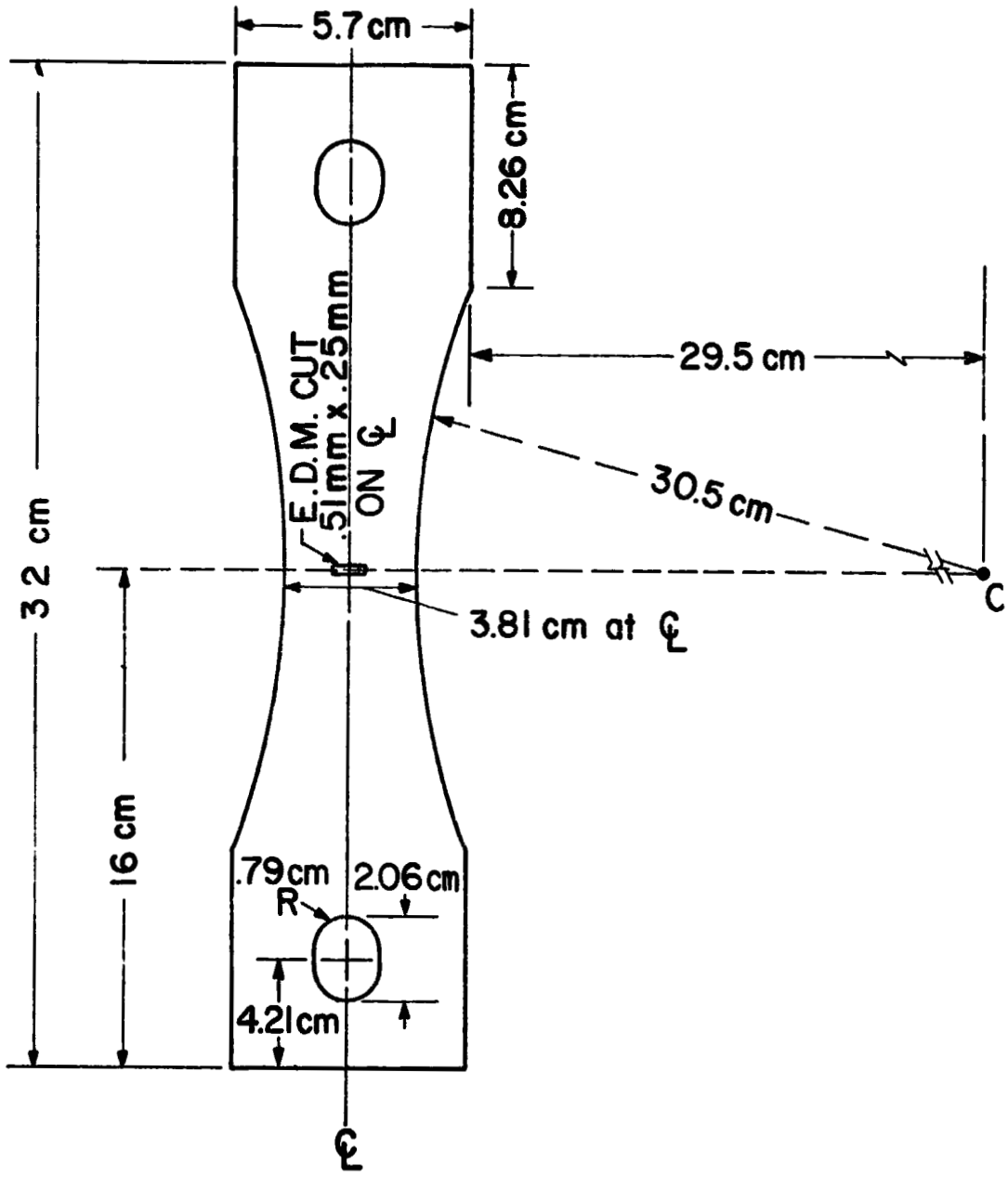

Figure 1.- Geometrical configuration of the fatigue specimen. The specimen is 2.28 mm thick. Figure not to scale.

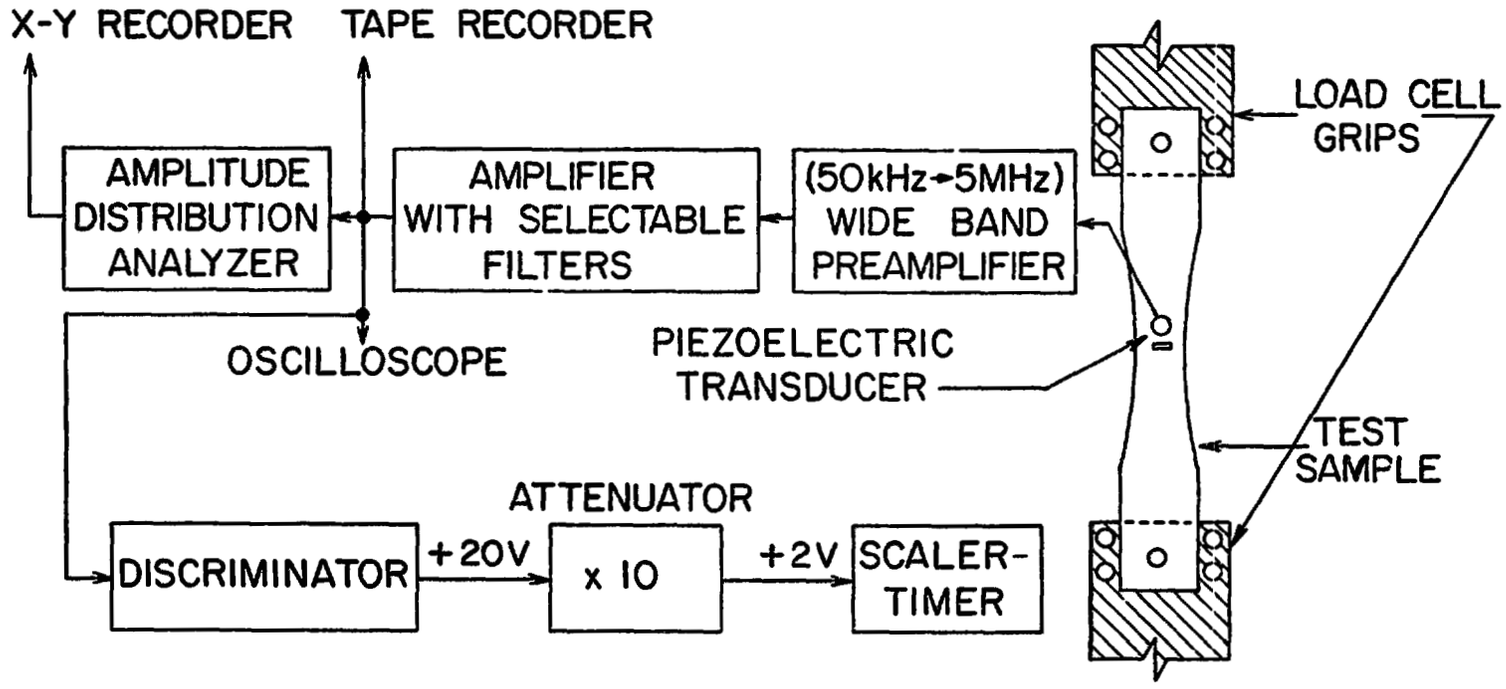

Figure 2.- Schematic diagram of the experimental setup used to record sound waves emitted by the test specimen.

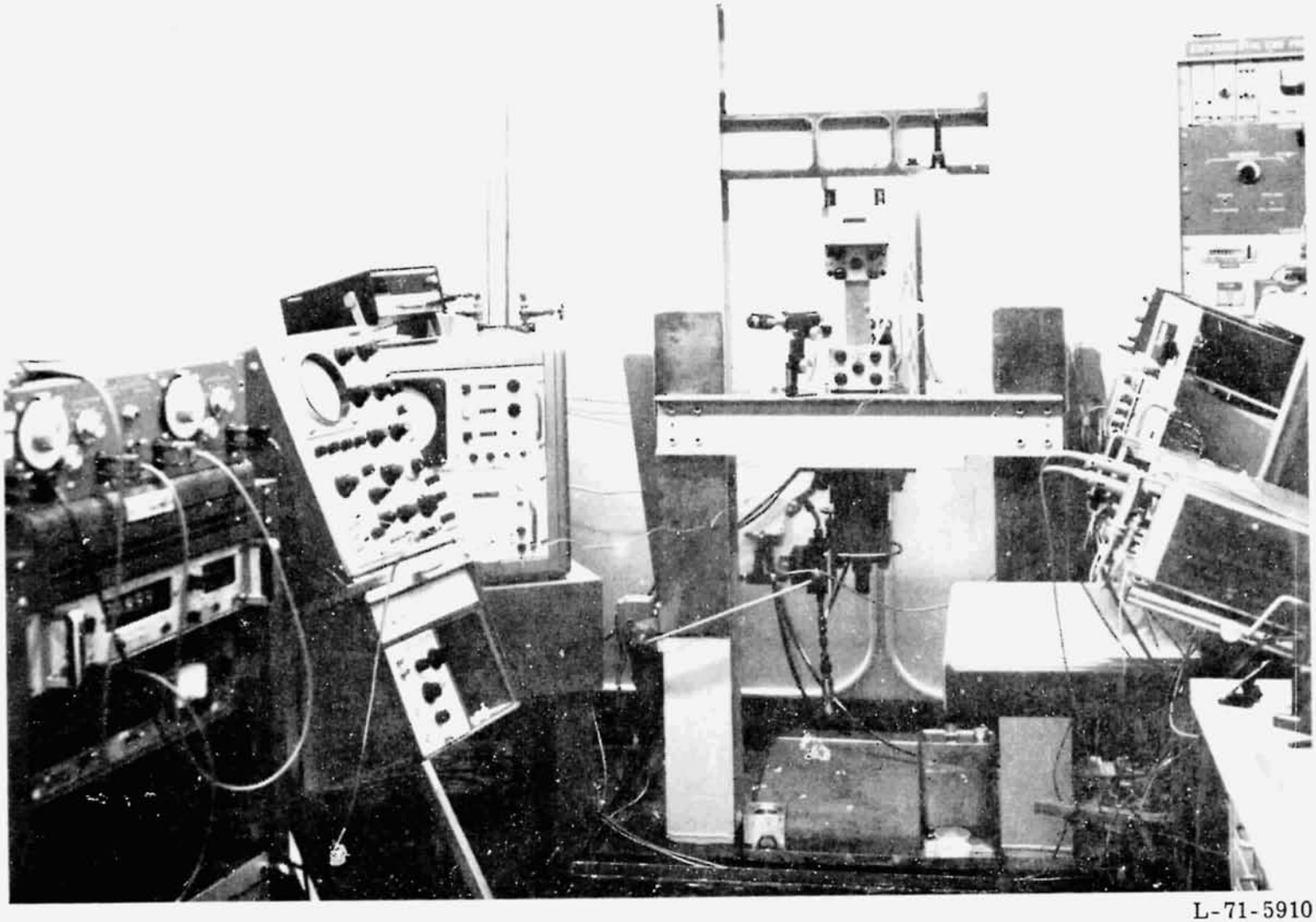

L-71-5910

Figure 3.- Photograph of the experimental setup.

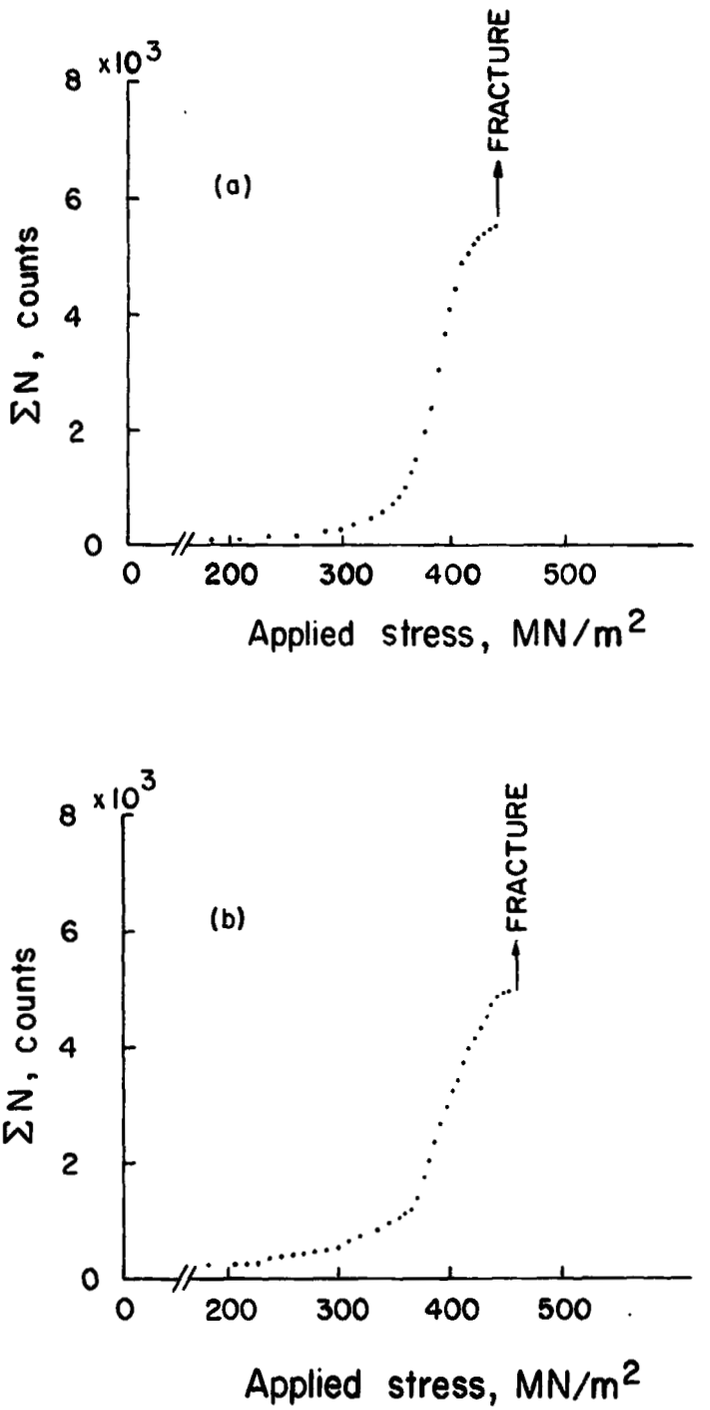

Figure 4.- Acoustic emission from an unflawed aluminum specimen statically loaded to failure.

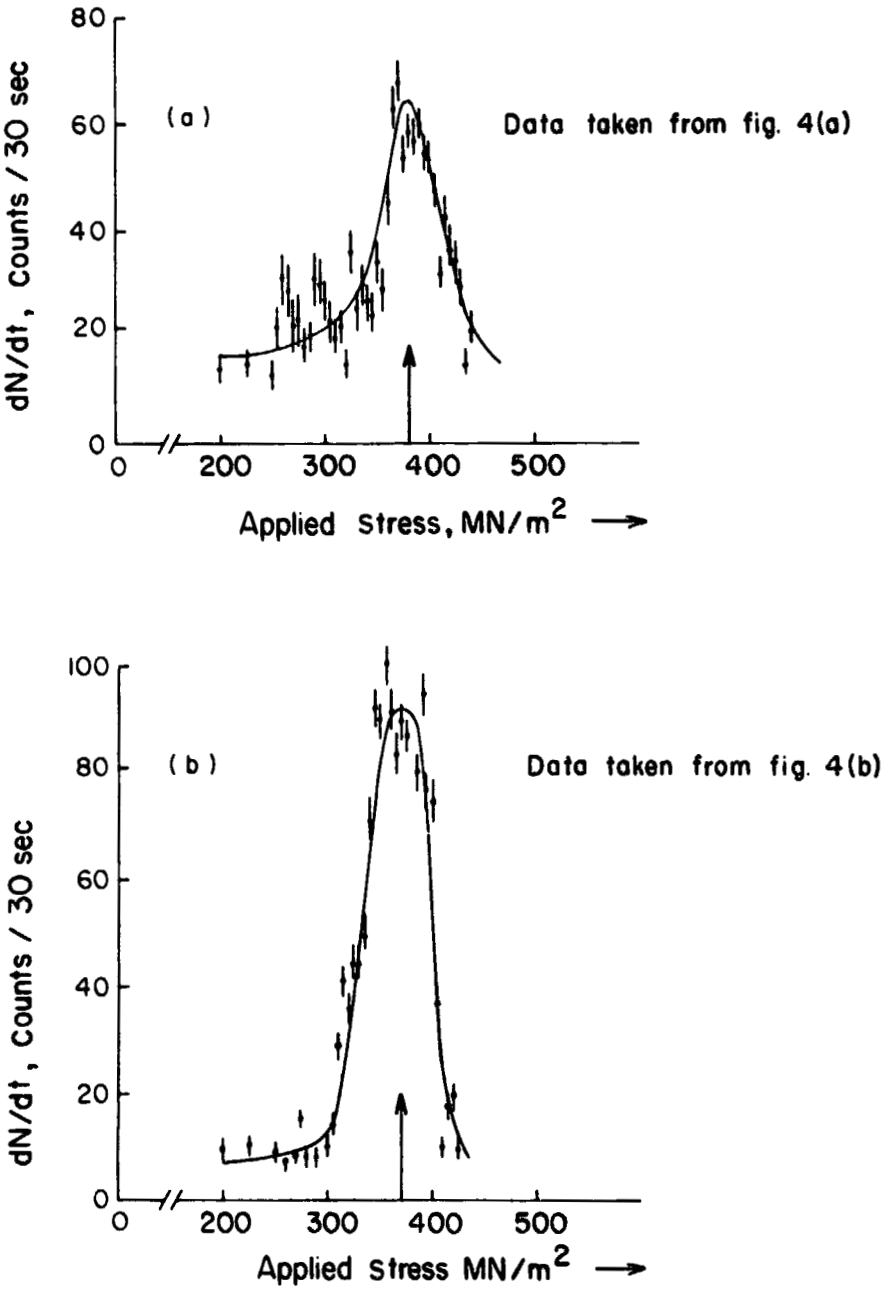

Figure 5.- Acoustic emission rate from an unflawed aluminum specimen statically loaded to failure.

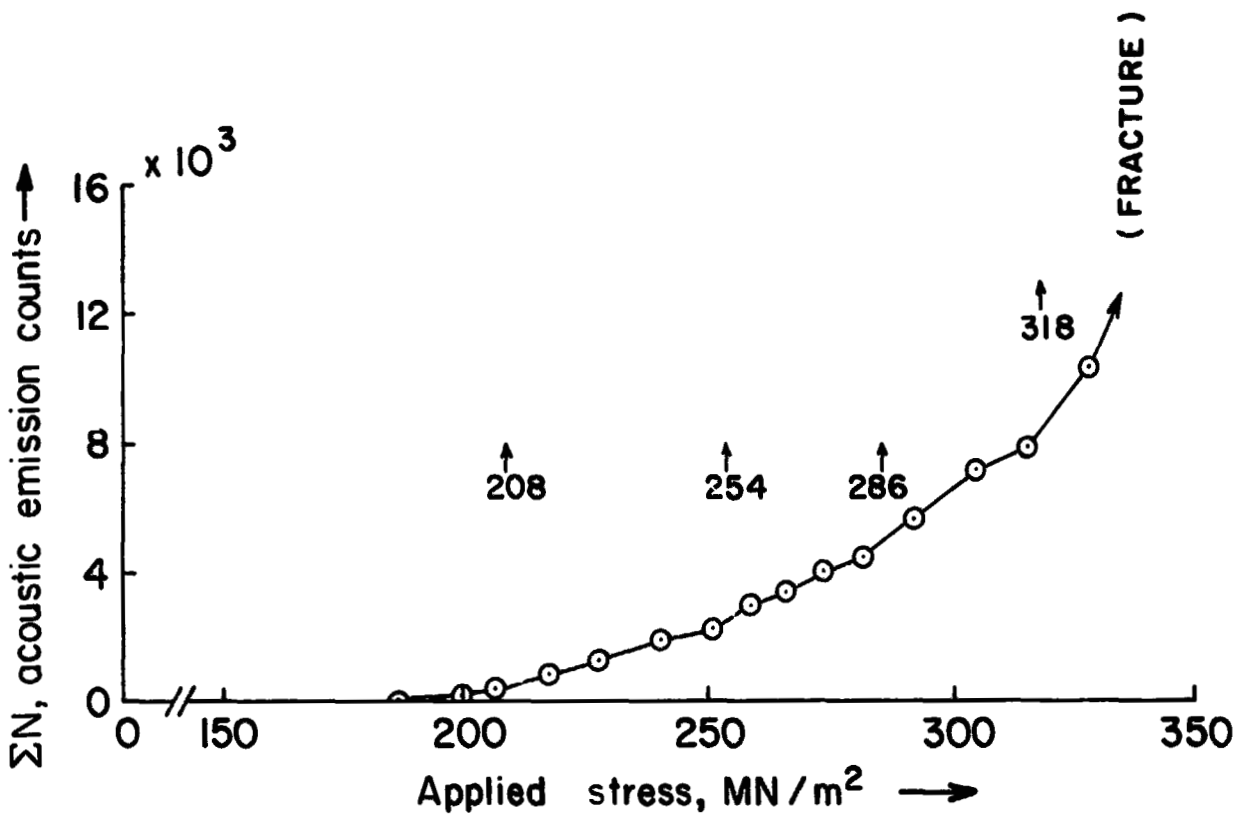

Figure 6.- Cumulative acoustic emission from an initially cracked specimen subjected to increasing tensile load. Initial crack produced by cycling at 5.2 to 186 MN/m^2; $(2a)_i = 4.57$ mm.

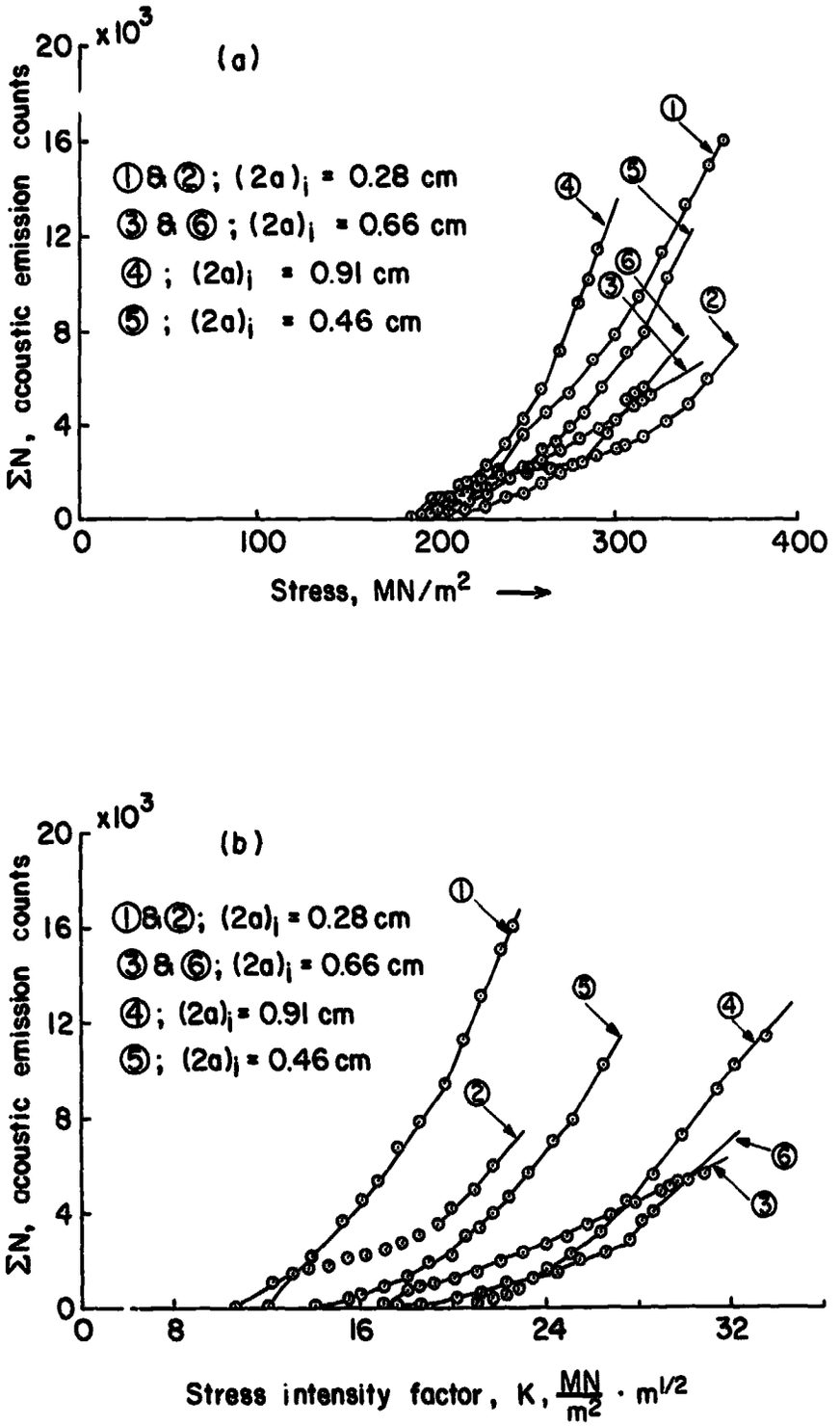

Figure 7.- Acoustic emission as a function of stress for six fracture specimens.

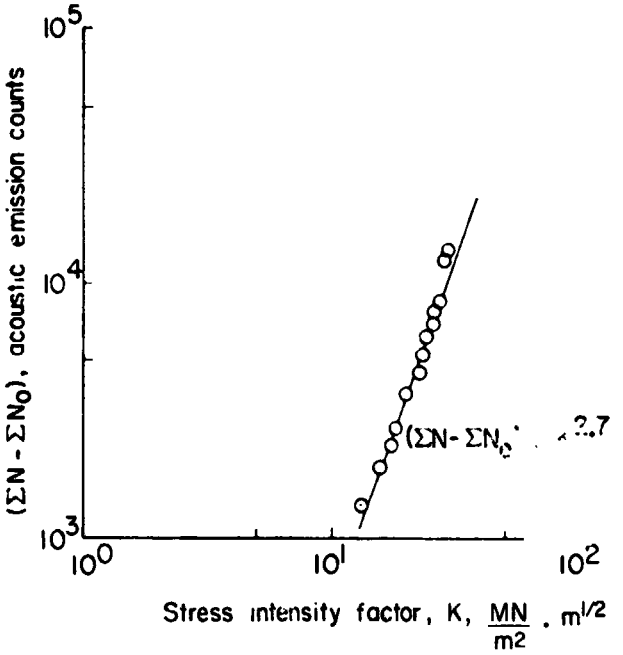

(a) $(2a)_i = 0.605$ cm.

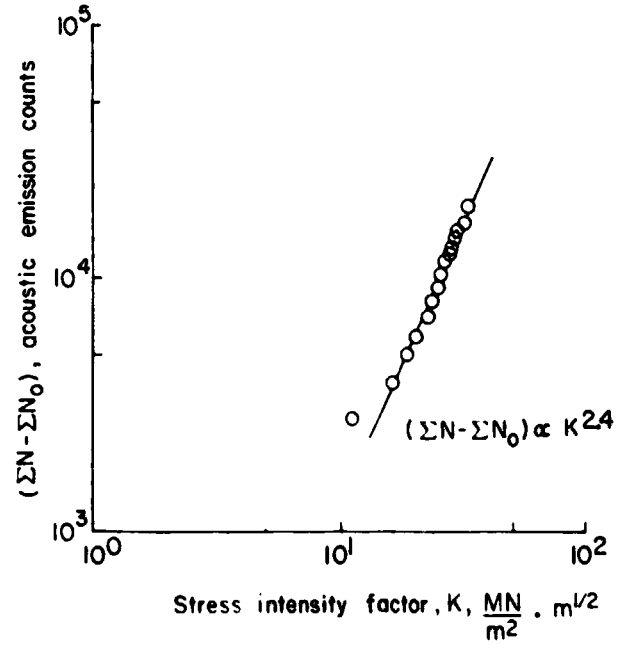

(b) $(2a)_i = 0.889$ cm.

Figure 8.- Summation acoustic emission as a function of stress intensity factor in statically loaded 2024-T3 Al plate specimen.

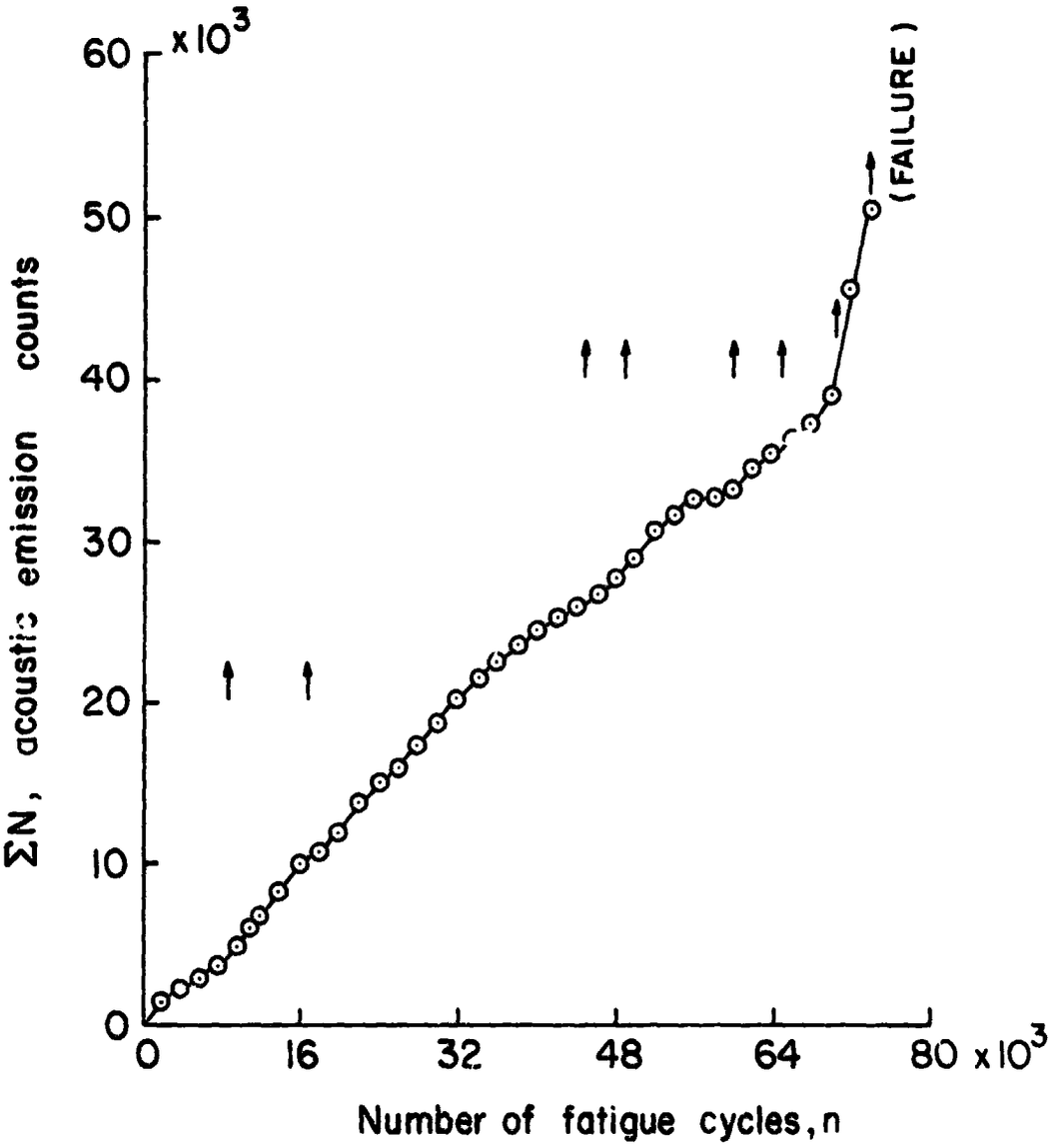

Figure 9.- Summation acoustic emission from an unflawed 2024-T3 Al specimen cycled at 5.2 to 160 MN/m^2 at 16 Hz.

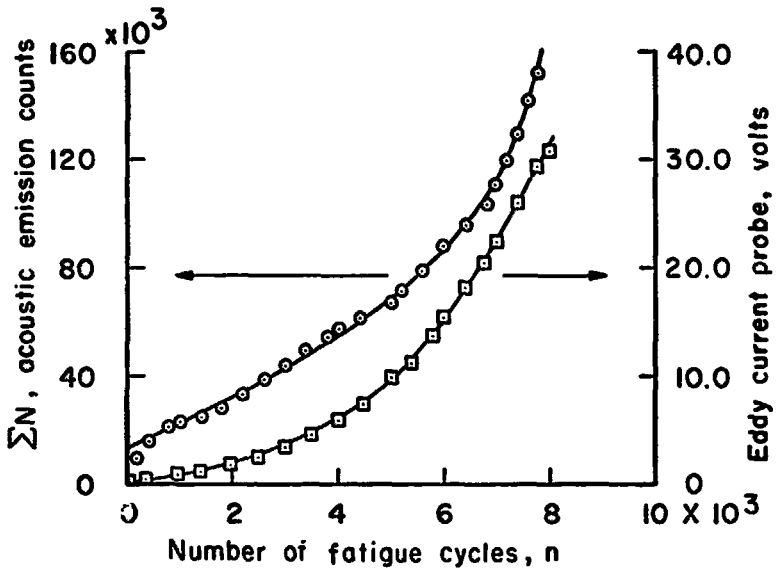

(a) Comparison between acoustic emission and eddy probe signal at various fatigue loads.

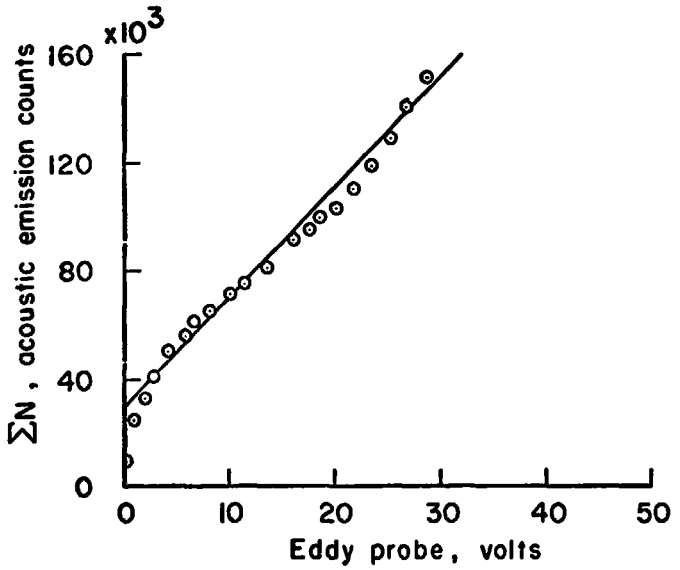

(b) Correlation between the acoustic emission and eddy probe signals.

Figure 10.- Correlation between acoustic emission and eddy probe signal in cyclically loaded 2024-T3 Al specimen; 5.2 to 104 MN/m^2 at 16 Hz.

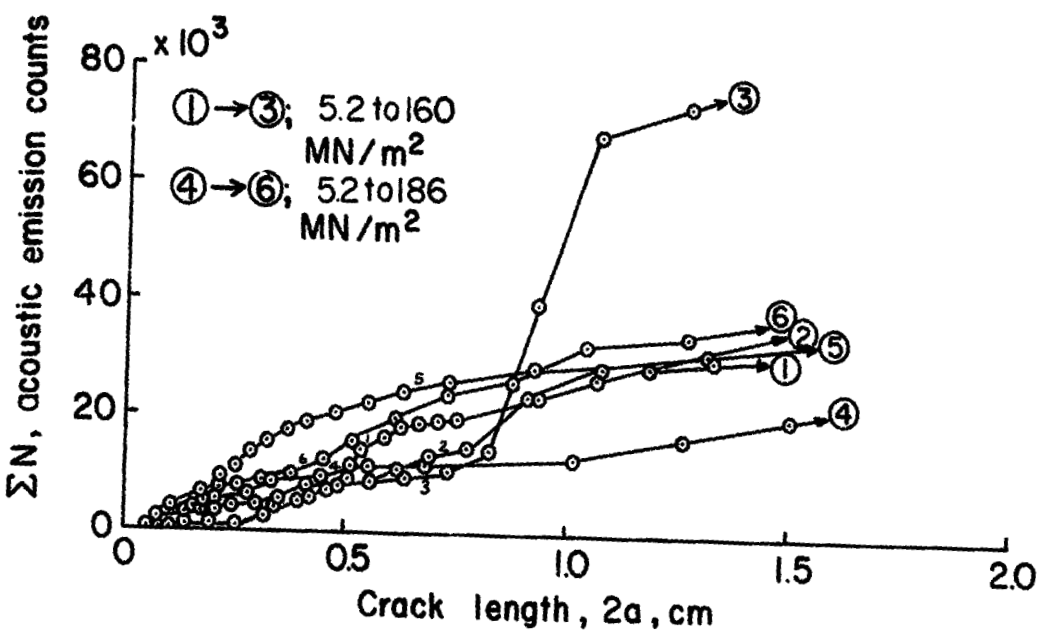

(a) Acoustic emission as a function of crack length.

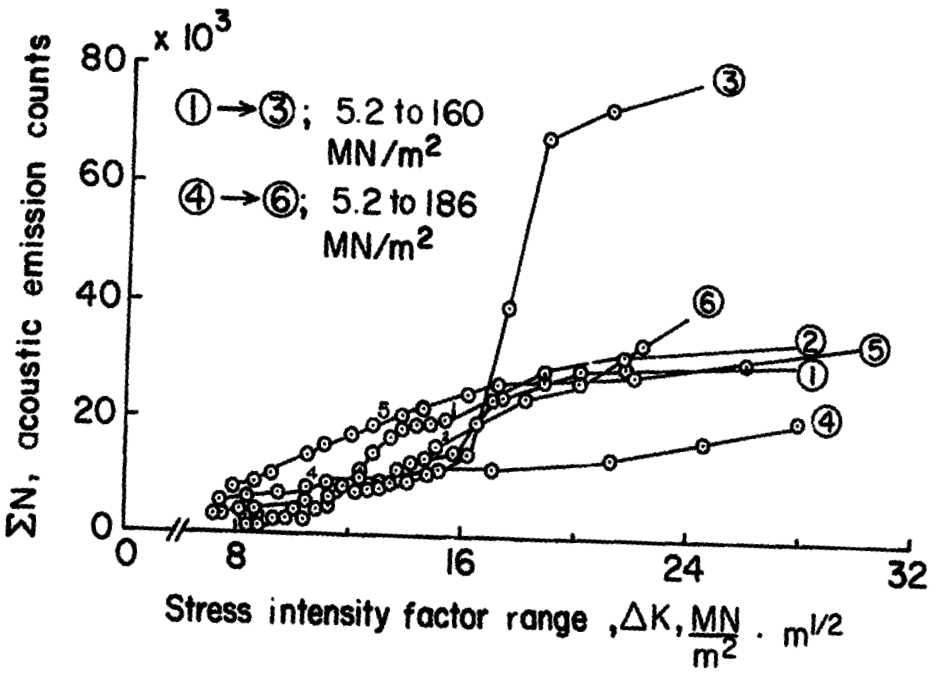

(b) Acoustic emission as a function of stress intensity factor range.

Figure 11.- Acoustic emission as a function of crack length and stress intensity factor range for six fatigue specimens.

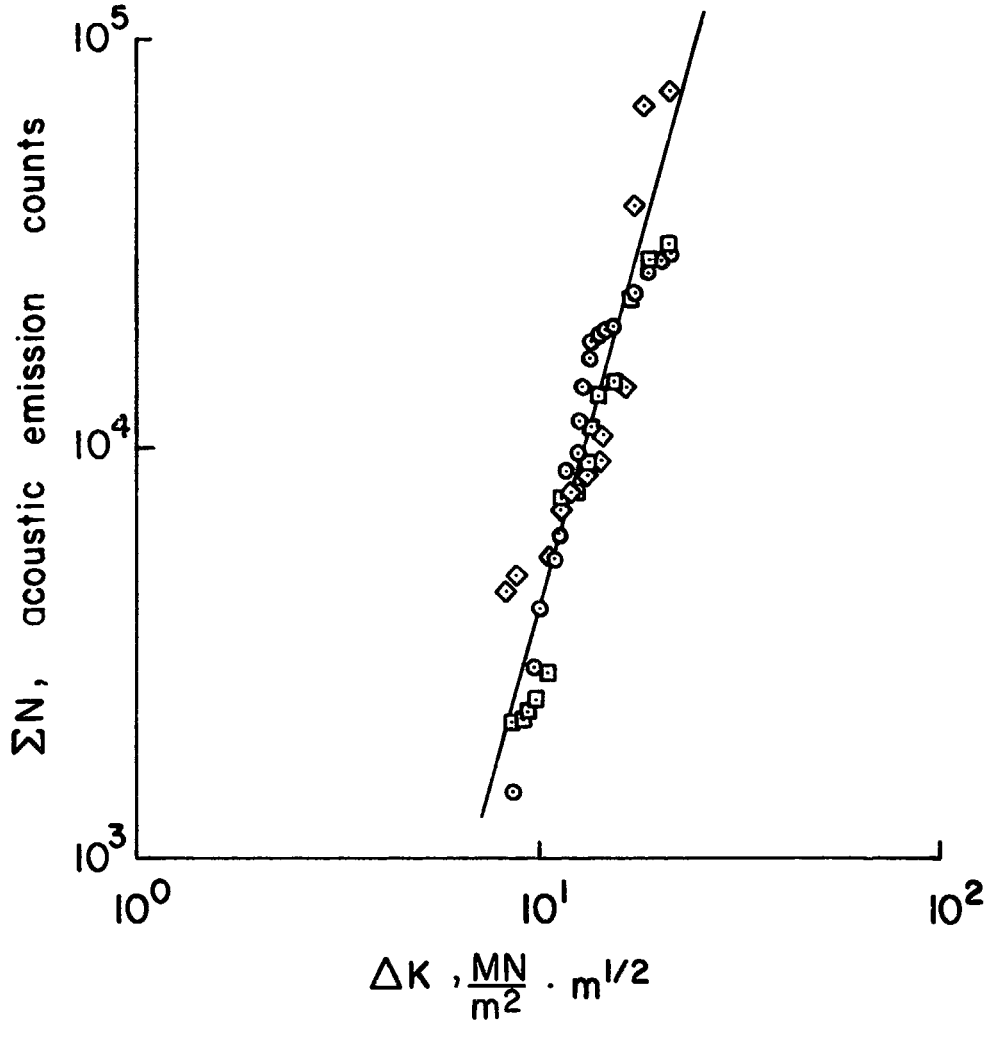

Figure 12.- Summary of ΣN plotted against ΔK at 5.2 to 160 MN/m^2 at 16 Hz. $\Sigma N \propto (\Delta K)^{2.5}$. Test points indicate the values obtained in three separate runs.

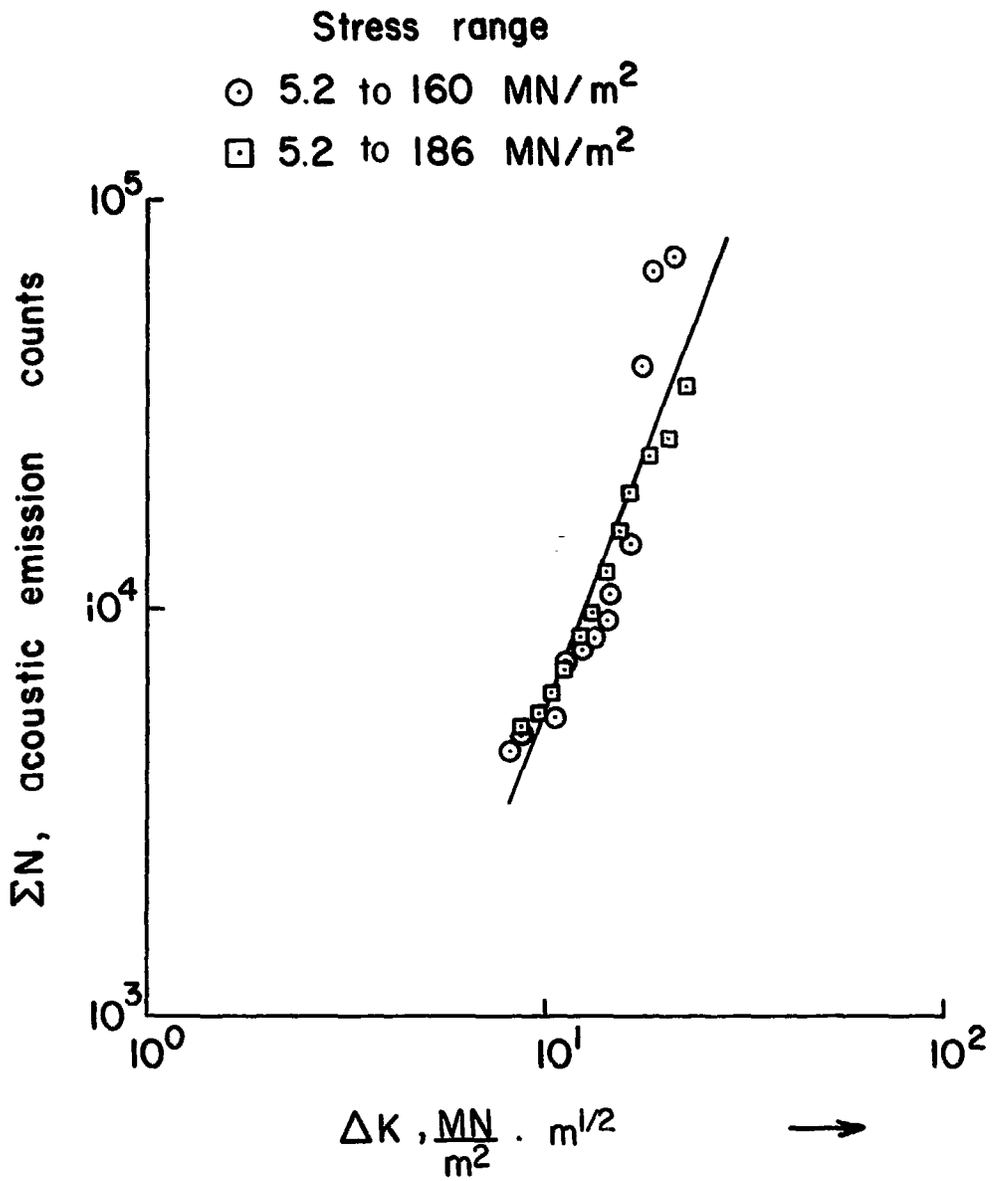

Figure 13.- Comparison of ΣN plotted against ΔK at two different load levels. $\Sigma N \propto (\Delta K)^{2.5}$.

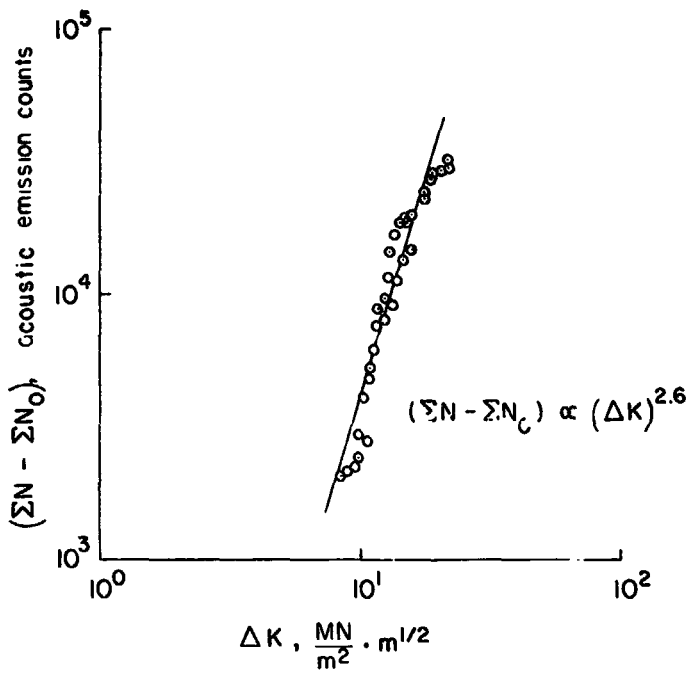

(a) At 5.2 to 160 MN/m^2.

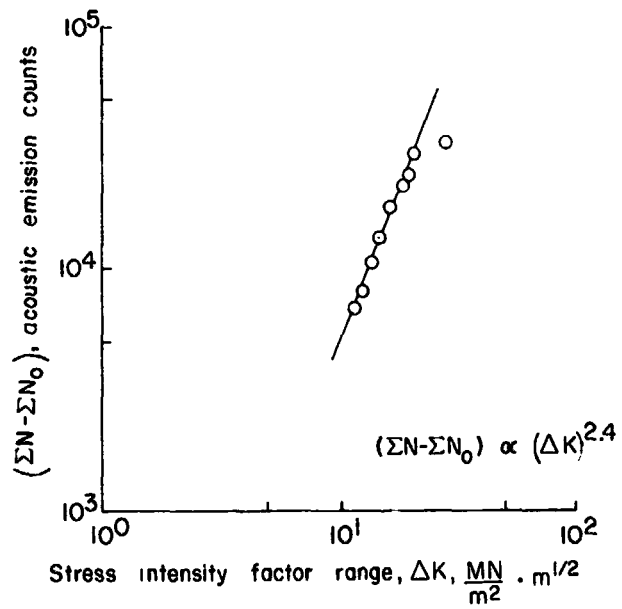

(b) At 5.2 to 186 MN/m^2.

Figure 14.- Summation acoustic emission as a function of stress intensity factor range in cyclically loaded 2024-T3 Al plate specimen.

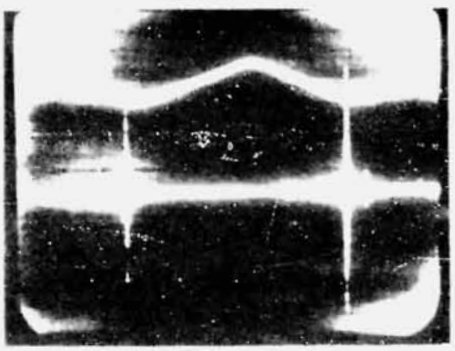

Stress cycle: 5.2 to 88 MN/m^2
Time base: 10 ms/div
Vertical scale (load): 2.0 volt/div
Vertical scale (signal): 0.2 volt/div

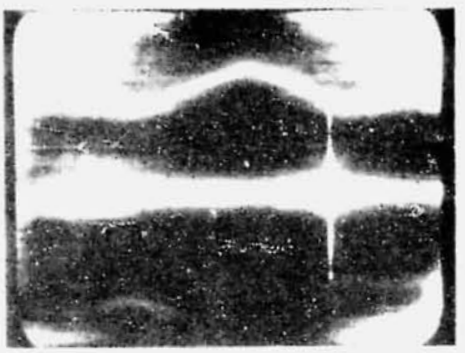

Stress cycle: 5.2 to 88 MN/m^2
Time base: 10ms/div
Vertical scale (load): 2.0 volt/div
Vertical scale (signal): 0.2 volt/div

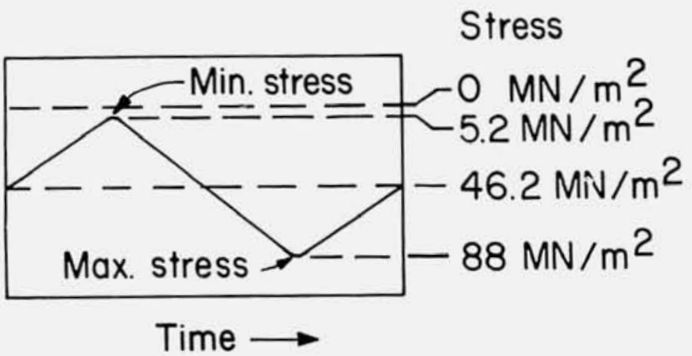

Schematic trace of the tension - tension stress cycle

L-74-1153

Figure 15.- Photographs of the oscilloscope screen showing the stress cycle, acoustic emission, and background signals including crack-closure and related noise.

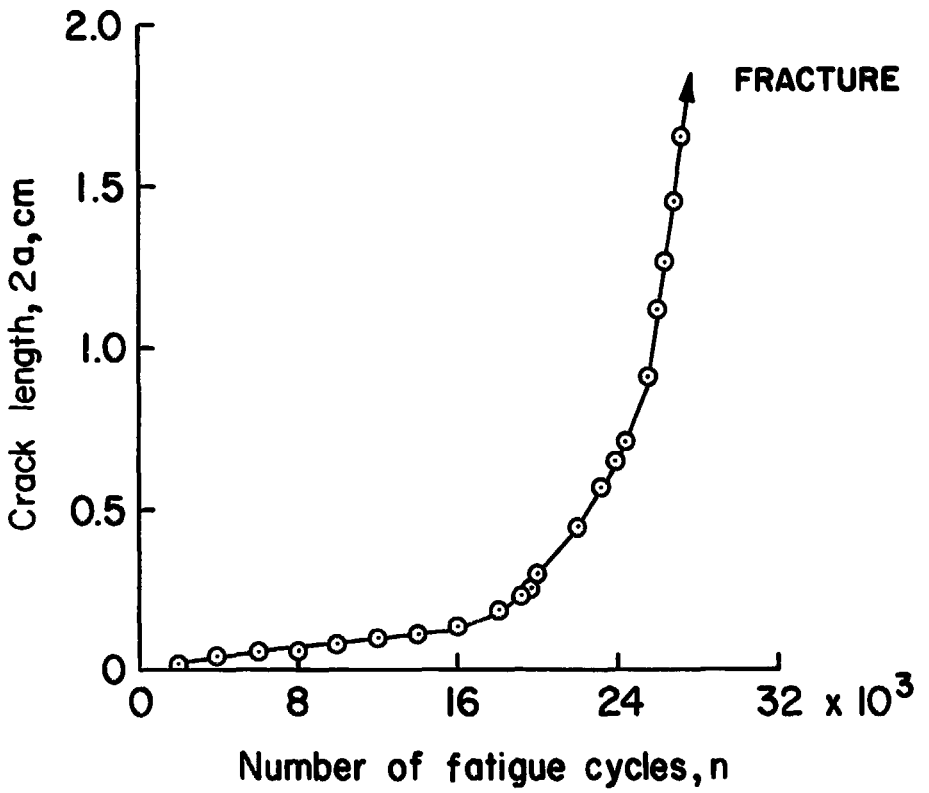

Figure 16.- Crack length as a function of fatigue cycles in a 2024-T3 Al specimen cycled at 5.2 to 186 MN/m^2 at 13 Hz.

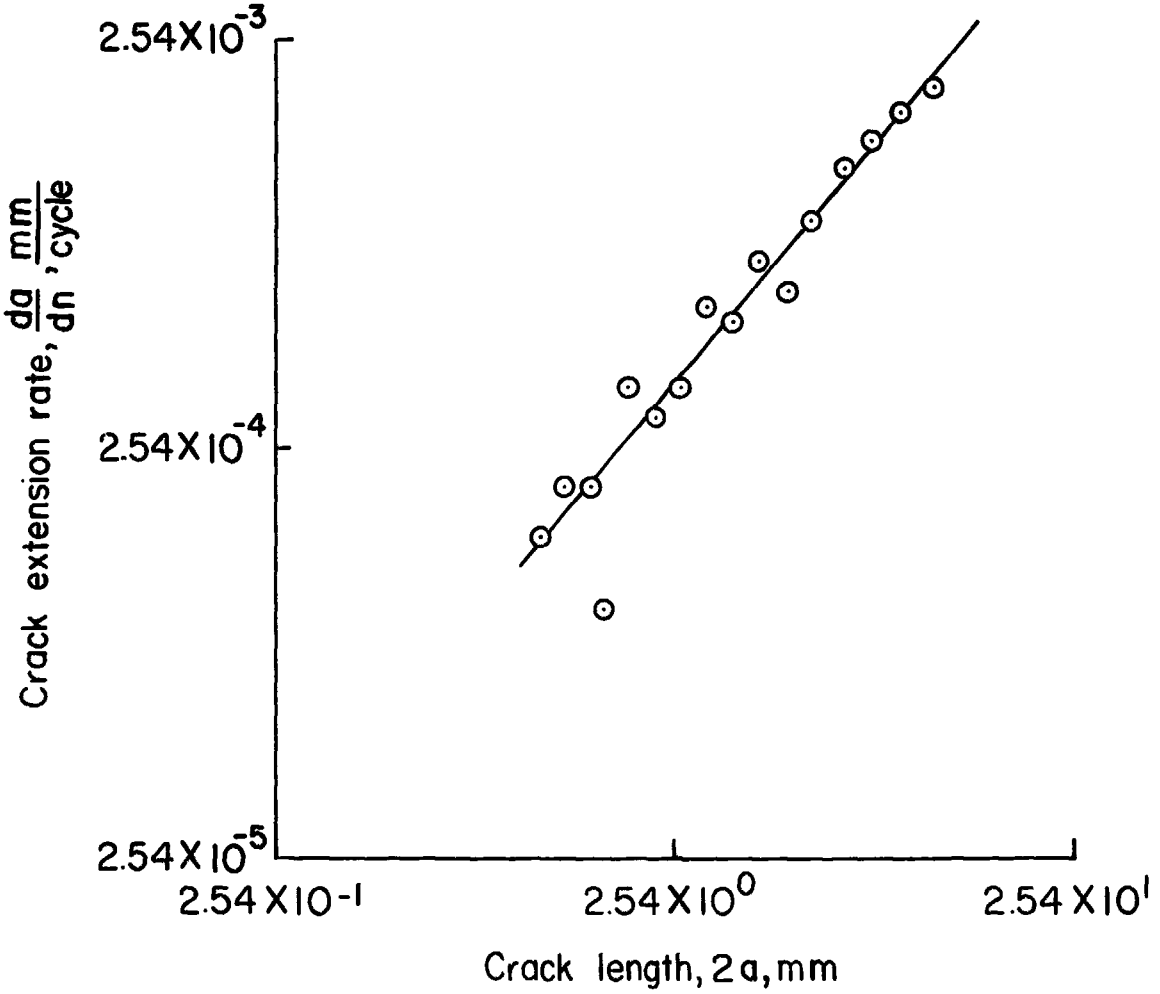

Figure 17.- Crack extension rate as a function of total crack length in cyclically loaded 2024-T3 Al specimen at 5.2 to 186 MN/m2. $\frac{da}{dn} \propto (2a)^{1.1}$.

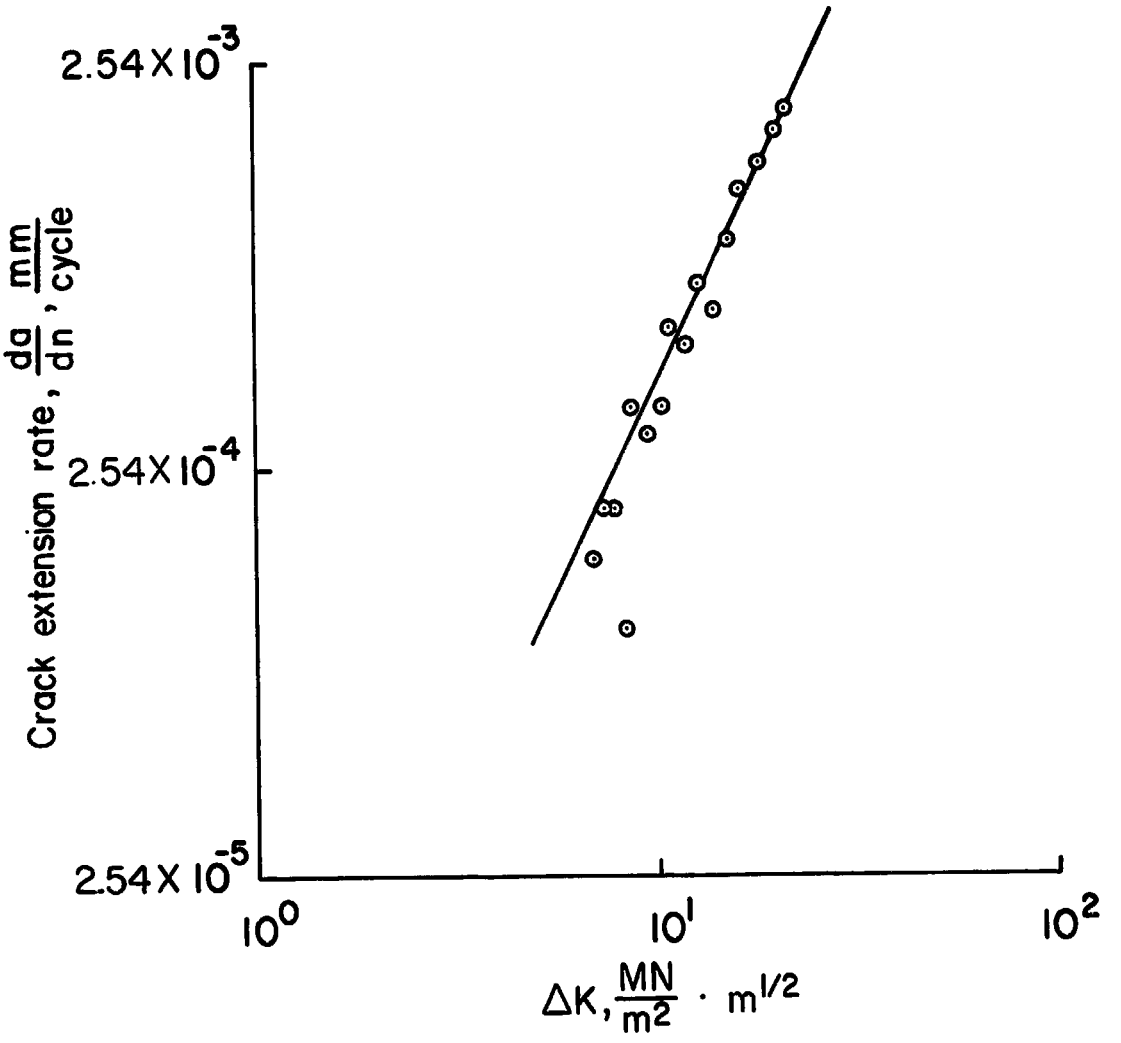

Figure 18.- Crack propagation rate versus stress intensity factor range in a 2024-T3 Al specimen cycled at 5.2 to 186 MN/m2. $\frac{da}{dn} \propto (\Delta K)^{2.4}$.

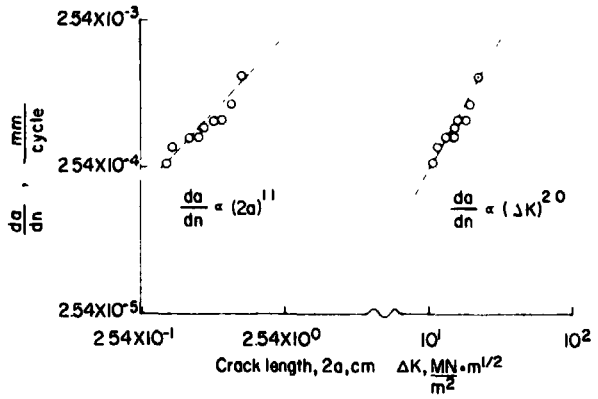

(a) Stress range: 5.2 to 160 MN/m^2.

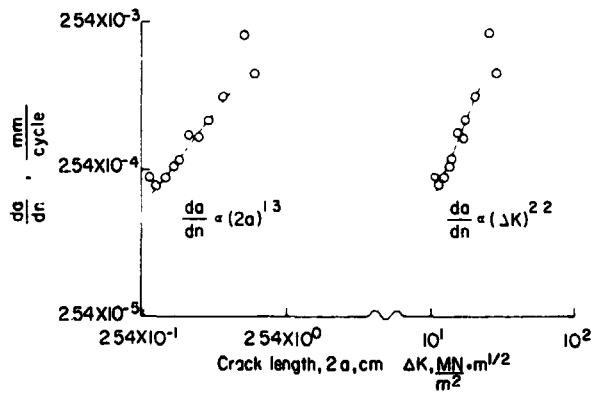

(b) Stress range: 5.2 to 186 MN/m^2.

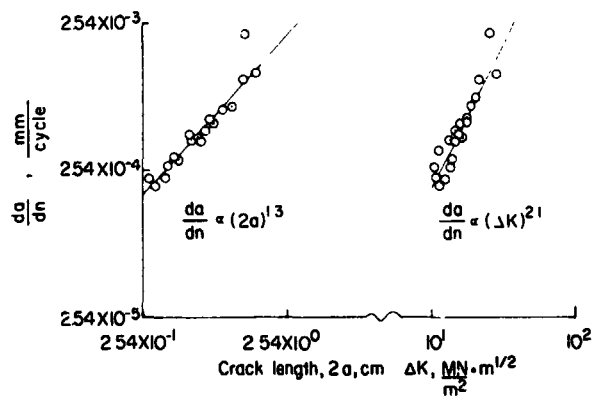

(c) Stress ranges: 5.2 to 160 MN/m^2; 5.2 to 186 MN/m^2.

Figure 19.- Comparison of da/dn plotted against 2a and da/dn plotted against ΔK at two different stress ratios in 2024-T3 Al specimen.

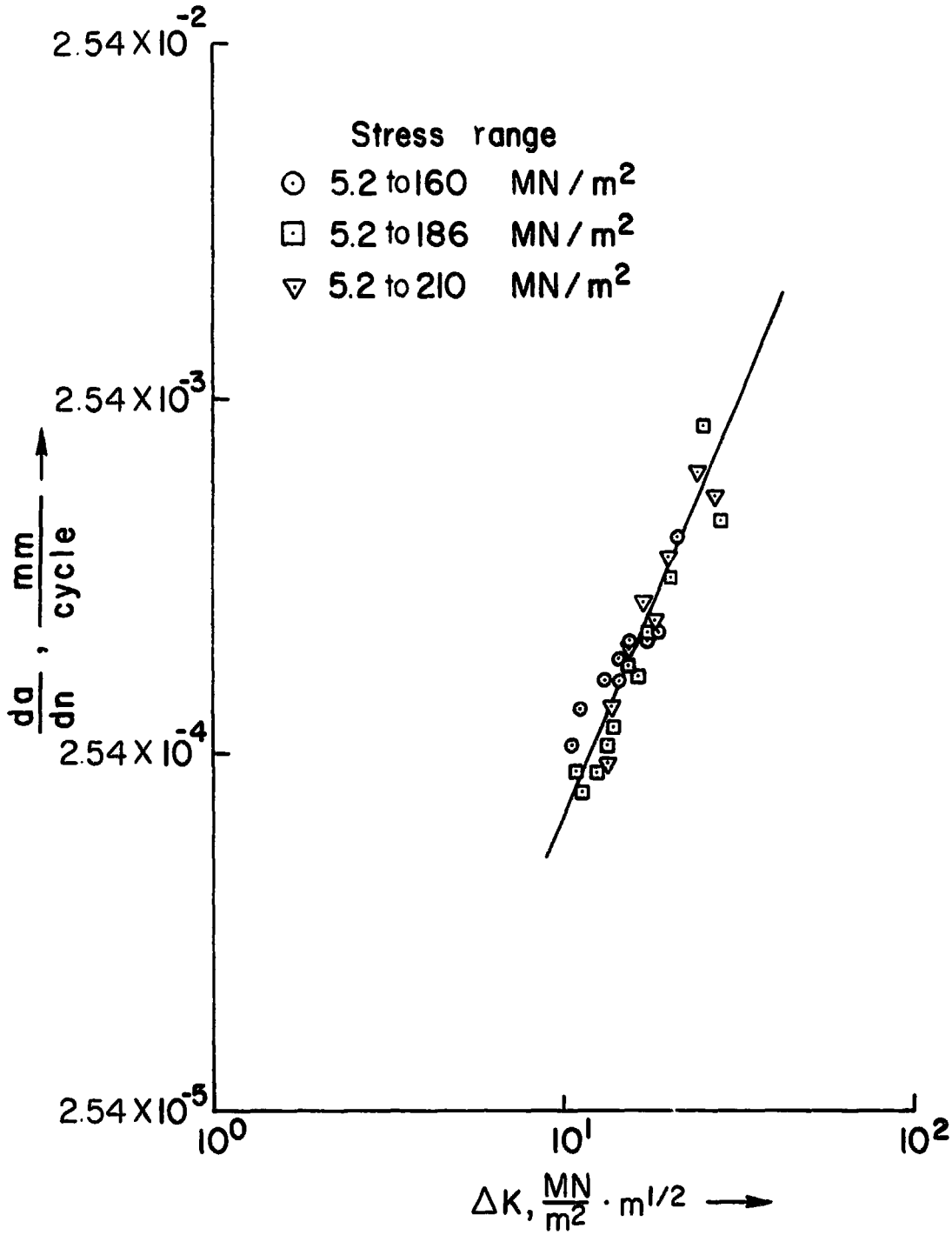

Figure 20.- Summary of results for da/dn as a function of ΔK at three different stress ratios in 2024-T3 Al specimen. $\frac{da}{dn} \propto (\Delta K)^{2.3}$.

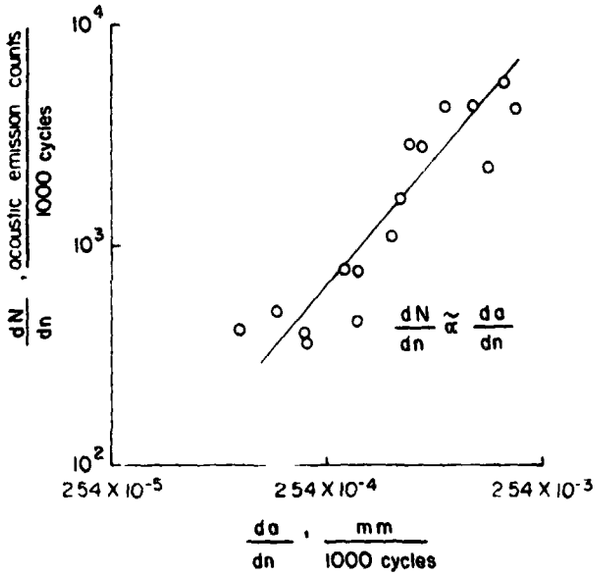

(a) Acoustic emission as a function of crack propagation rate. Stress range, 5.2 to 186 MN/m2.

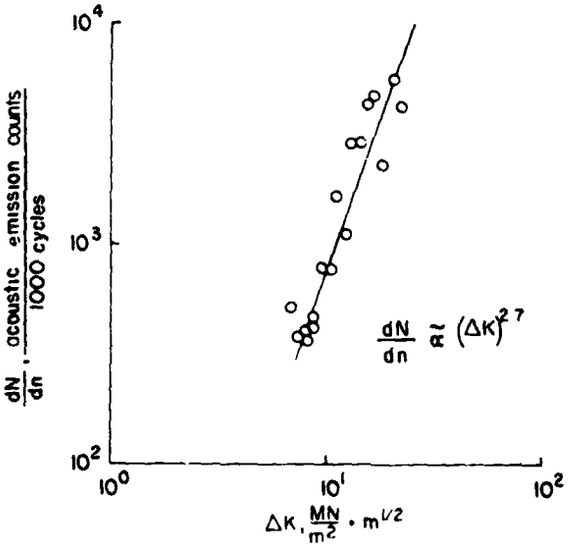

(b) Acoustic emission as a function of stress intensity factor range. Stress range, 5.2 to 186 MN/m2.

Figure 21.- Acoustic emission rate in cyclically loaded 2024-T3 Al specimen.

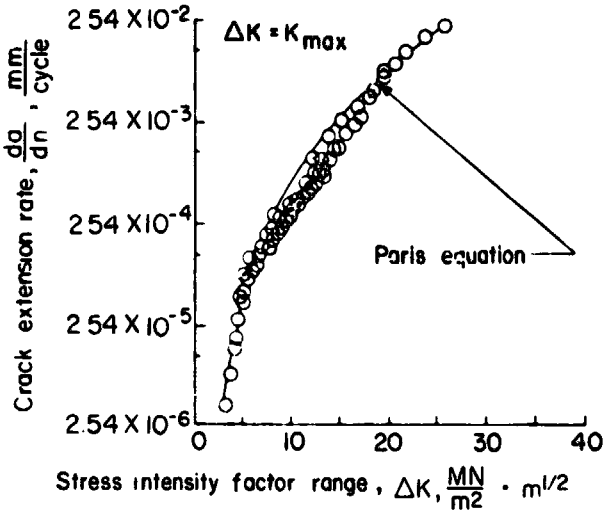

(a) Comparison of experimental fatigue crack growth rates with Paris equation. (The data for this figure have been taken from ref. 16.) $\frac{da}{dn} \quad (\Delta K)^{4.0}$.

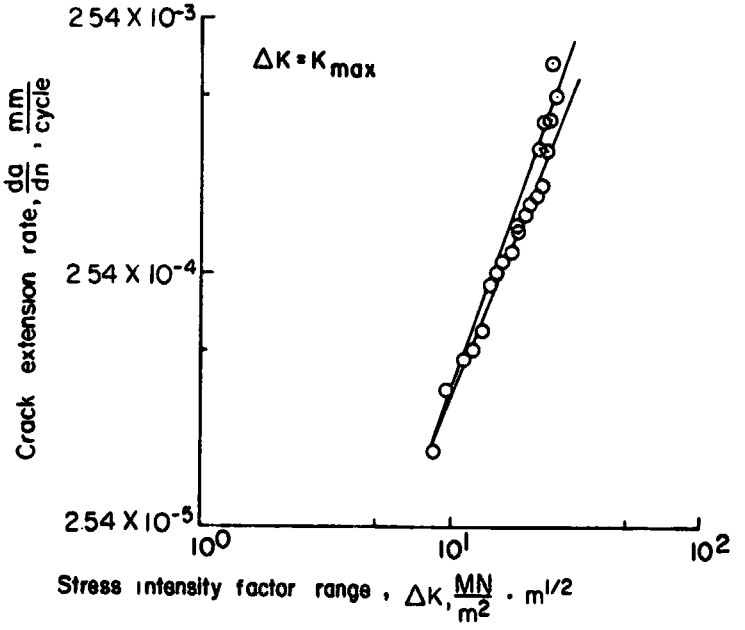

(b) Fatigue crack growth rate as a function of stress intensity factor range in 2024-T3 Al specimen. (These data have been taken from the critical region of fig. 22(a).) $\frac{da}{dn} \propto (\Delta K)^{2.4\text{-}3.0}$.

Figure 22.- Fatigue crack growth rate as a function of stress intensity factor range.

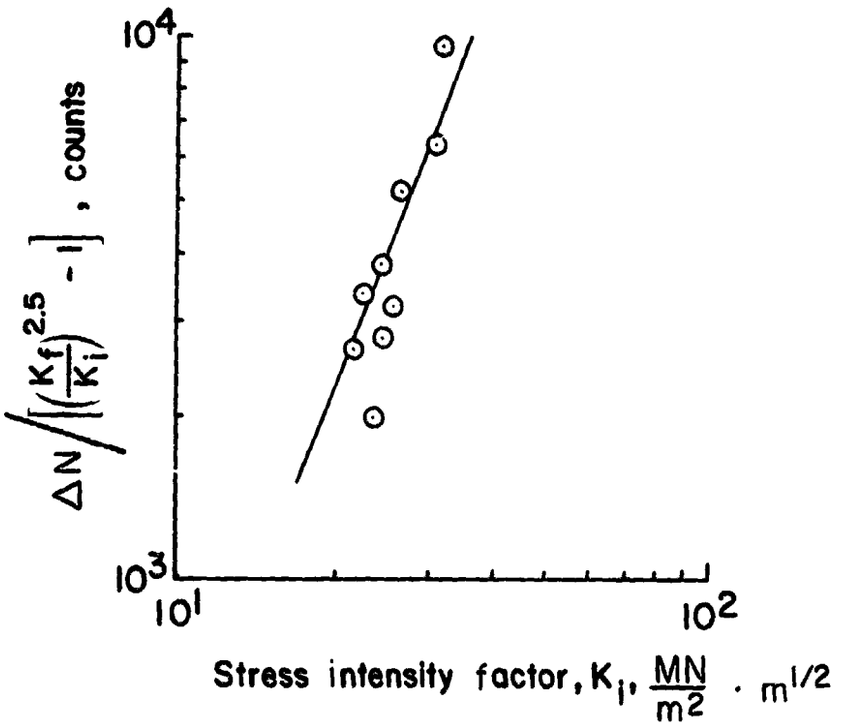

(a) Normalized acoustic emission counts as a function of initial stress intensity factor in the proof test of flawed 2024-T3 Al specimen. $\frac{\Delta N}{\left(\frac{K_f}{K_i}\right)^{2.5} - 1} \cdot K_i^{2.5}$.

Figure 23.- Variation of acoustic emission counts.

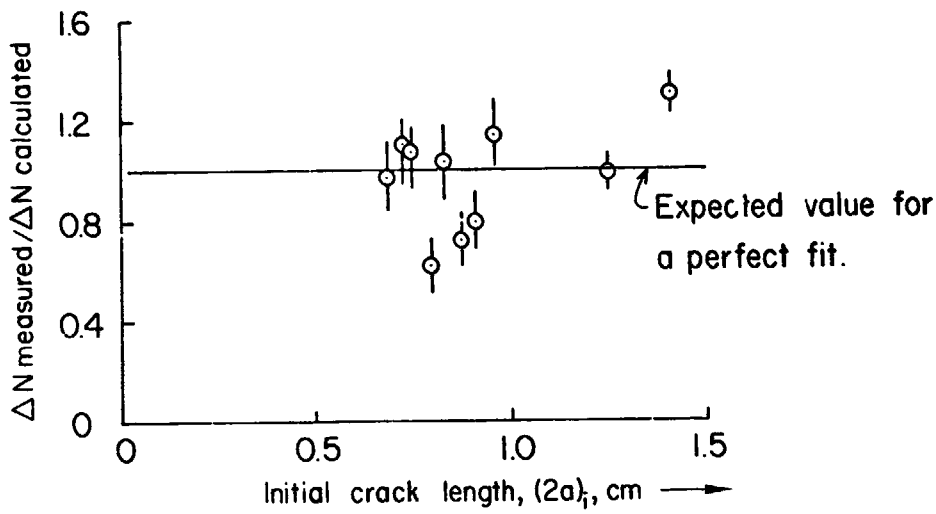

(b) Comparison of the observed and computed proof acoustic counts.

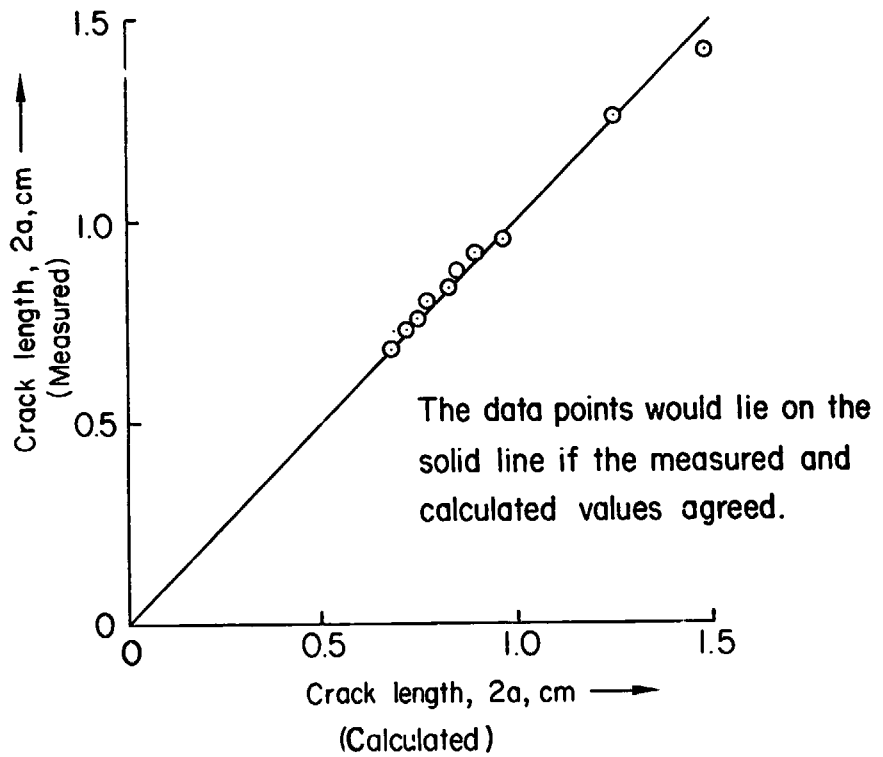

(c) Comparison of the measured and the calculated crack lengths.

Figure 23.- Concluded.